Chapter 3
Physical-Chemical Methods of Nanocomposite Synthesis

On the whole, methods of production of nanostructural materials can be divided in two groups: physical and chemical. However, this separation is conditional, because, for example, all physical methods contain considerable chemical component, and it is often difficult to draw a distinct boundary between different methods. Special character of physical methods, prevailingly vapor phased, is in formation of crystal nanoparticles with vast open surface, which advances formation of strong aggregates, difficultly parted into primary particles. Moreover, it is often impossible to obtain complex phases because of their segregation at high temperatures typical of gas phase processes. A special place has methods, in which nanoparticles form as a result of different "physical" impacts, for example, under ultrasonic or microwave radiation. This effect stimulates different processes in a reaction mixture, first of all, chemical reactions, which brings to formation of nanostructural material with a definite composition, structure and properties. Therefore, these methods are often related to intermediate physical-chemical group.

Most physical-chemical methods of production of nanoparticles are based on homogeneous nucleation in vapor phase or heterogeneous nucleation in contact with surface, followed by condensation and coagulation. A necessary condition for condensation from the vapor phase is supersaturation, which can be reached by physical or chemical methods. Depending on a character of the heating processes (resistive, laser, plasma, electric arc, induction, ionic) and cooling, different methods of production of nanomaterials are distinguished, such as flame pyrolysis (see Chap. 7), synthesis in a flow reactors, laser induced evaporation and pyrolysis, thermal and microwave plasma methods, laser ablation. This group also includes solvo-thermal synthesis, pyrolysis of aerosols, and most methods of growth of nanoparticles and films from vapor phase, for example, chemical deposition from vapor phase (CVD), etc. Many of these methods are rather well described in literature, there are voluminous reviews and monographs [1–5]. Below only most typical methods are considered, which, in our opinion, are of keen interest for production of nanocomposite materials.

A.D. Pomogailo, G.I. Dzhardimalieva, *Nanostructured Materials Preparation via Condensation Ways*, DOI 10.1007/978-90-481-2567-8_3

3.1 Synthesis of Nanocomposites by Microwave Irradiation

Prospects of using of microwave energy in development of nanocomposite materials are determined by a possibility of bulk heating of materials. As is shown in Chap. 2, methods of chemical reduction often include complex and continuous reactions of molecular precursors in presence of solvents, ligands and/or surfactants at elevated temperatures. Microwave heating has some advantages as compared to conventional methods of heating of condensed matters, in particular, high rate and low inertia of heating, uniformity of heating of material over the volume, and, as a consequence, decrease in thermal stress and high homogeneity of microstructure of the obtained composites, etc. Owing to this, microwave radiation is widely used in synthesis of nanocrystalline materials. General information about microwave heating of dielectric materials, criteria of estimation of efficiency of its usage in different processes of organic synthesis, polymer chemistry, materials science, nano- and biotechnology, etc. are described in reviews [6–9].

3.1.1 Basic Principals

Microwave radiation is non-ionizing electromagnetic radiation at frequencies from 300 MHz to 30 GHz. Most experimental studies are performed at the frequency of electromagnetic radiation 2.45 GHz (Fig. 3.1).

If a substance is under impact in the range of microwave frequencies, its dipoles are oriented along applied electric field. Oscillation of the field causes re-orientation of bipolar molecules, which try to follow alternate electric field, which is accompanied by energy loss due to molecular friction and dielectric loss.

Scattering of microwave irradiation power per unit volume in a material can be expressed by equation:

$$P = c|E|^2 f\varepsilon'' = c|E|^2 f\varepsilon' \tan\delta \tag{3.1}$$

where c is the constant, E is the intensity of electric field, f is the radiation frequency, ε'- imaginary part of equivalent dielectric permeability of a substance, and ε'' – real part, $\tan\delta = \varepsilon''/\varepsilon'$ – dielectric loss tangent.

There is optimal frequency range of dielectric loss coefficient, which determines absorption ability of a matter. On the whole, media with high tgδ are characterized by high absorption ability and, respectively, efficiency of heating (Table 3.1).

In the synthesis of nanocrystalline materials a wide range of solvents is used: with strong (for example, ionic liquids, ethylene glycol), intermediate (water, methyl pyrrolidone) absorption abilities, and also media almost transparent for microwave radiation (non-polar alkanes or alkenes), i.e. the substances should have either high coefficient of dielectric loss tangent (they should have mobile dipoles with rather high dipole momentum), or high ion, electron, or hole conductivity.

Water, alcohols, DMF, ethylene glycol have high dielectric loss tangent and are ideal for microwave heating (Table 3.2).

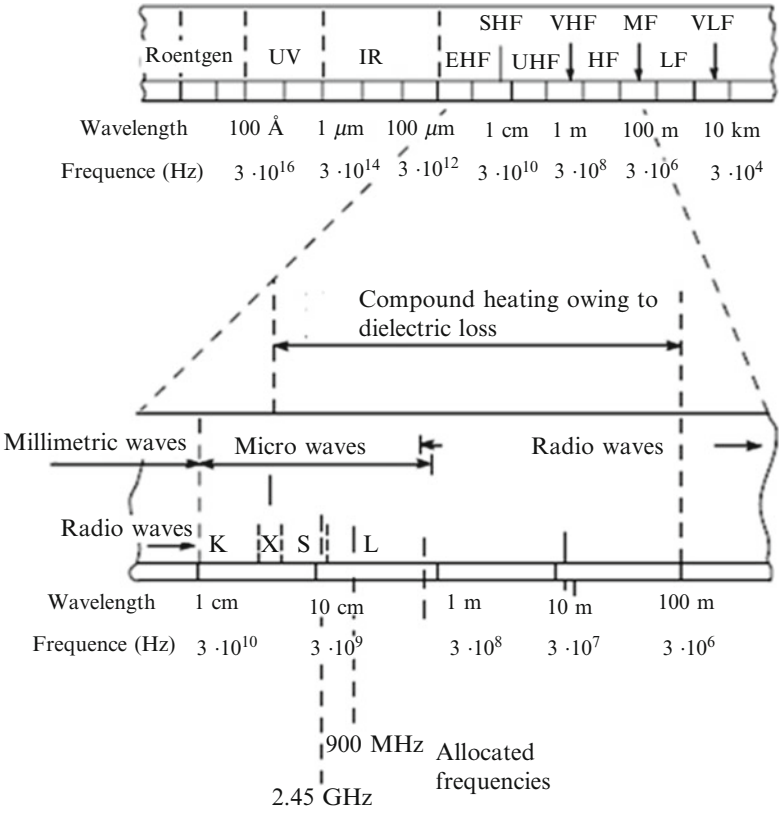

Fig. 3.1 Microwave electromagnetic irradiation scale

Table 3.1 Dielectric loss tangent (tanδ) for different solvents [6]

Solvent	tanδ	Solvent	tanδ
Ethylene glycol	1.350	DMF	0.161
Ethanol	0.941	1,2-dichloroethane	0.127
DMSO	0.825	Aqua	0.123
2-Propanol	0.799	Phenyl chloride	0.101
Formic acid	0.722	Acetonitrile	0.062
Methanol	0.659	Acetone	0.054
1,2- dichlorobenzene	0.280	Tetrahydrofuran	0.047
N-methyl-2- pyrrolidone	0.275	Dichloromethane	0.042
1-butyl-3- methylimidazolium hexafluorophosphate	0.185	Toluene	0.040
Acetic acid	0.174	Hexane	0.02

The processes in microwave field may be intensified by non-thermal effects of microwave radiation. Main approaches to grounding of the mechanism of non-thermal effect consider acceleration of diffusion processes [10, 11], some authors relate these phenomena to surface polarization [12].

Table 3.2 Physical parameters of typical solvents used for microwave heating [7].

Solvent	T_{boil}, °C	ε'	ε''	tanδ
Aqua	100	78.3	12.3	0.157
Methanol	65	32.7	20.9	0.639
Ethanol	78	24.3	6.08	0.200
N,N-dimethylformamide	153	36.7	–	–
Ethylene glycol	198	41.0	41.0	1.00
N-methyl-2-pyrrolidone	202	32.0	8.855	0.277

3.1.2 Microwave Heating in Synthesis of Colloid Nanocrystals

It should be noted that most experiments with microwave radiation are confined to simple "one-pot" schemes with one-step heating, when all reacting substances presence in the initial reaction mixture and are heated to a given temperature. In this case it is impossible to use, for example, such well-known procedures as "hot-injection" for separation of nucleation and growth stages, or to conduct consequent addition of selective reagents to control particle size distribution and shape. Under microwave radiation so called "heating-up" technique is used, when reagents mixed at environmental temperature are rapidly heated to high temperature. This scheme is especially efficient in colloid systems in which super saturation point is a limiting stage [13]. Monomer precursors can form in shape of intermediates during slow reaction or during decomposition of quite stable monomer-surfactant complexes. Thus, complex formation of poly(vinylpyrrolidone) with Ag^+ ions before the beginning of microwave heating advances reduction predominantly on polymer chains, and a polymer molecule additionally inhibits cluster aggregation at early stages of the reaction, which on the whole favors formation of narrow dispersed distribution of nanoparticles [14]. Specific impact of microwave irradiation can manifest itself in increase in reduction ability of a reducing agent, as was observed in polyethylene glycol [15] or glutathione [16] and $AgNO_3$ system. It is interesting to note that under comparable conditions, but at ordinary convection heating for 24 h no reaction products were found. Analogous effect of microwave irradiation was found in carboxymethylcellulose-Na_2PtCl_6, $HAuCl_4$ $3H_2O$ or $PdCl_2$, systems, in which noble metals are reduced only under conditions of microwave heating at 100 °C [17], no reducing agents or stabilizers were required.

Formation of different polygonal nanoplates (triangular, square, pentagonal and hexagonal) was observed at microwave heating (198 °C) during reduction of $HAuCl_4$ in ethylene glycol and in presence of PVP [18]. At the same time heating in oil bath to the same temperature causes formation of prevailingly spherical particles of 100—190 nm in diameter and a small fraction of rod-shaped nanoparticles. This difference in character of formation of nanostructures is, probably, caused by explosive nucleation owing to fast homogeneous dielectric heating, which cannot be reached under conditions of ordinary heating. Thus, microwave heating allows conducting of hydrothermal synthesis of ferrite [19] or perovskite [20–22] nanoparticles at lower temperatures and shorter times, which manifests itself in substantial decrease in sizes

Table 3.3 The effect of reaction conditions on sizes of ferrite nanoparticles [19]

Sample	Reaction conditions	Grain size by XRD data, nm	Nanoparticle size by TEM data, nm	Morphology
$NiFe_2O_4$, $CoFe_2O_4$, $MnFe_2O_4$	Ordinary hydrothermal heating, 250 °C, 1 h; the ratio oleic acid/ iron nitrate 3:1, 6:1	7 ± 1	9 ± 1	Spherical
	Ordinary hydrothermal heating, 250 °C, 2 h; the ratio oleic acid/ iron nitrate 3:1, 6:1	7 ± 1	9 ± 1	Spherical
	Ordinary hydrothermal heating, 250 °C, 2 h; the ratio oleic acid/ iron nitrate 3:1, 6:1	7 ± 1	9 ± 1	Spherical
	Microwave heating, 160°C, 1 h	3.5 ± 1	5 ± 2	Spherical
	Microwave heating, 160 °C, 2 h	6.5 ± 1	9 ± 1	Spherical
γ-Fe_2O_3	Ordinary hydrothermal heating, 120 °C, 1 h; the ratio oleic acid/ iron nitrate 3:1	9 ± 1	10 ± 1	Spherical and cubic
	Ordinary hydrothermal heating, 120 °C, 1 h; the ratio oleic acid/ iron nitrate 3:1	4 ± 1	5 ± 1	Spherical

of formed nanoparticles and in increase in crystallization rate by one-two orders, than under conditions of ordinary hydrothermal synthesis (Table 3.3). In the case of perovskite dielectric ceramic materials this happens due to high absorption of electromagnetic radiation by these materials having high dielectric constants [23].

It is shown that advantages of microwave – polyolic synthesis of Ni nanoparticles as compared to traditional polyolic technique bring to increase in efficiency of the process and thus facilitate its scaling [24]. Microwave polyolic synthesis is very efficient for producing two- and three-component nanometer chalcogenides (selenides and tellurides) and can serve as a general way of their fabrication [25–28]. As it was noted in Sect. 2.2, polyols (such as ethylene glycol and other glycols) on the one hand, play the role of reducing agent and solvent in the processes of synthesis of metal nanoparticles, and, on the other hand, are very sensitive to microwave radiation due to high dipole moment and high dielectric loss tangent. Moreover, reducing properties of ethylene glycol are most efficient at high temperatures and, as is known, high-boiling solvents are less susceptible to carbonizing due to appearance of arc discharge. Besides, it should be noted that this phenomenon may be used as simpler and quite efficient method for production of metal/carbon composites with core-shell structure in organic solvents. Under conditions of microwave arc discharge, as a rule, highly organized carbon structures form, for example, graphene layers and Fe/C core-shell in nanocomposite obtained from toluene solution $Fe(CO)_5$-$C_{60/70}$ [29].

Increase in energy of microwave radiation effectively decreases reaction time and sizes of formed structures, which, probably, is caused by the fact that at higher energies a greater number of nuclei form, and this, provides a precursor concentration is the same, brings to a decrease in diameters of the particles [30], a decrease in role of

side effects, an increase in reaction yield, and improvement of reproducibility of the reactions [31]. And the observed increase in reaction rate is purely thermal/kinetic effect, i.e. it is a consequence of high temperature of the reaction, super-heated solvent above boiling temperature. Especially effective these processes go in media, highly absorbing microwave radiation, in particular, in ionic liquids. It is interesting that just impact of microwave heating causes decomposition of 1-butyl-3-methylimidazolium tetrafluoroborate used as ionic solvent during synthesis of Cu and Ni with formation of carbon, which in turn serves as a reducing agent and protective shell for the formed metal particles [32]. In this case, depending on irradiation time, the products of reduction for copper nitrate were Cu_2O or Cu for 5-min or 10-min microwave treatment in solution of ionic liquid, respectively. It should be noted that advantages of microwave heating, which provide uniform heating and equal rates of achievement of necessary temperature are very attractive for implementation of various reduction processes in hetero-metal systems, for example, for producing of core-shell structures or nanoparticles of metal alloys [33].

It is assumed that non-isothermal effects caused by absorption of long-chained molecules of polymer surfactant can advance formation of coarse anisotropic structures [7] (Scheme 3.1):

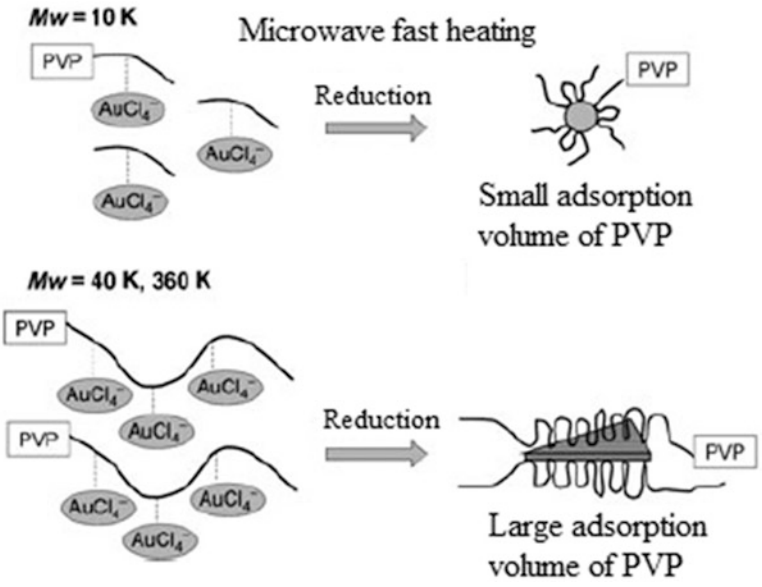

Scheme 3.1 Formation scheme of Au nanostructures using PVP with different chain lengths

Moreover, under conditions of microwave radiation transformation processes of nanoparticle shape are also possible. For example, coherent surface heating of silver particles stabilized by PVP brings to transformation from spherical Ag crystals into coarse prismatic particles, probably by Ostwald ripening mechanism [34].

3.2 Photo Chemical Reduction

Producing of metal nanoparticles under impact of high energies on chemical system is associated with generation of high-active strong reducing agents like electrons, radicals, excited particles. Typical wavelengths and energy ranges of the used electromagnetic radiations are shown in Table 3.4.

Methods of production of nanoparticles can be divided by the type of impact of input energy on chemical system as: photochemical (photolysis, < 60 eV), radiolytic (radiolysis, 60–10^4 eV), irradiation by fast electron flow ($>10^4$ eV). Ionizing radiation is generated by a source of X-rays and gamma rays, ultraviolet and visible irradiations are usually generated by a mercury vapor lamp, or by xenon lamp. Among the special features of chemical processes induced by high-energy irradiation there are the following: high volume and surface energy density; non-equilibrium state, which manifests itself in non-Maxwell, non-Boltzmann functions of particle size distribution and population of quantum energy levels; approaching and overlap of typical τ times of physical, physical-chemical and chemical processes; the leading role in chemical transitions of highly reactive particles; multichannel character and instability of the processes in a reacting system (Table 3.5).

A number and size of formed nanoparticles can be controlled due to regulation of intensity of flow of electromagnetic radiation quanta, which are able to efficiently and rapidly stimulate reduction reactions.

3.2.1 The Main Approaches to the Synthesis of Matrix-Stabilized Nanoparticles by Photochemical Irradiation

Photo and radiation-chemical reduction has some advantages as compared to chemical reduction. Stimulated by radiation reduction reactions can be carried out in different media, including solid ones (for example, polymer matrices, films) and at low temperatures with good reproducibility. In parallel to this it is

Table 3.4 Scale of electromagnetic waves

Radiation	λ, nm	*E*, eV
Fast electrons	–	$>10^4$
Gamma and X-ray:		
Hard	0.2–100	$6.2 \cdot 10^3$–12.4
Soft radiation	>100	<12.4
Ultraviolet:	10–400	124–3.1
Deep (vacuum)	10–200	124–62
Near radiation	200–400	62–3.1
Visible light	400–700	3.1–1.67

Table 3.5 Some physical-chemical characteristics of irradiation impact

Characteristic	Methods		
	Photolysis	Radiolysis	Fast electrons
Active reactive particles	Electron-vibrating-excited molecules, ions, and electrons	Electrons, ions, electron-excited particles	Electrons, ions, electron excited particles
Initial processes	$h\nu + M \rightarrow M^* \rightarrow$ Products	$e^-, h\nu + M \rightarrow M^+, e^-, (M^+)^* \rightarrow$ Products	$e^- + M \rightarrow M^+, M^*, (M^+)^* \rightarrow$ Products
Hierarchy of typical times of a process	$\tau_v < \tau_{ch} \leq \tau_e$	$\tau_{ch} \approx \tau_{dif}$	$\tau_{ch} \approx \tau_{tr}$
Generation rate of reactive particles ($v \cdot 10^{-15}$, cm^3/s)	10^{-2}–10^{-3}	~10^{-3}	~$2 \cdot 10^4$

Legend: *ch* chemical reaction, *v* vibrating relaxation, *e* electron relaxation, *tr* transport, *dif* diffusion

possible to obtain quite chemically pure target products without impurities, in particular accompanying chemical reduction methods. Duration of irradiation can be a simple experimental criterion for control over sizes of the formed particles [35], though in some cases increase in exposure time causes an increase in yield of nanoparticles, and has insignificant effect on their size [36].

At the same time, methods combining chemical and photochemical reduction, when a reducing agent also presents in a system [37, 38], are quite widely spread. A good example is photochemical reduction of $HAuCl_4$ in water media containing ethylene glycol of different concentrations and in presence of poly-4-vinylpyrrolidone. Mechanism of this reaction is studied in detail in [39]. As it was mentioned in Sect. 2.3, ethylene glycol is widely used as a reducing agent and viscous solvent slowing down diffusion in polyol processes of nanoparticles fabrication. However, these reactions as a rule are performed at high temperatures (160–280 °C), in order to reach reduction of metal ions. Continuous UV radiation of the ion metal salt under conditions of the considered reaction caused formation of nanoparticles at room temperature. Increase in rate of Au^{3+} extinction (absorption band at 323 nm in UV/visible range of the spectrum) during irradiation and in formation rate of nanoparticles (up to 0.4 mol fraction of glycol), as well as regeneration of Au^{3+} and its repeated disappearance some time later, and increase in intensity of a plasmon resonance band in a dark phase signs that ethylene glycol participates in the reduction reaction. The proposed mechanism took into account the role of ethylene glycol not only in reduction of excited Au^{3+}, but, probably, in reactions of Au^{2+} with Au^+:

$$Au^{3+}Cl_4^- \xrightarrow{h\nu} \left[Au^{3+}Cl_4^-\right]^* \tag{3.2}$$

$$\left[Au^{3+}Cl_4^-\right]^* \overset{\text{glycol}}{\rightarrow} Au^{2+}Cl_3^- + Cl^- \tag{3.3}$$

$$2Au^{2+}Cl_3^- \rightarrow Au^{1+}Cl_2^- + Au^{3+}Cl_4^- \tag{3.4}$$

$$4\,Au^{1+}Cl_2^- \rightarrow 2Au^{2+}Cl_3^- + 2Au^0 + 2Cl^- \tag{3.5}$$

$$3Au^{1+}Cl_2^- \rightarrow Au^{3+}Cl_4^- + 2Au^0 + 2Cl^- \tag{3.6}$$

$$Au^{m+} \overset{\text{glycol}}{\rightarrow} Au^0 (m+ \ : \ 3+, \ 2+, \ 1+) \tag{3.7}$$

$$nAu^0 \rightarrow Au^0 + \left(Au^0\right)_n \tag{3.8}$$

As a mole fraction of ethylene glycol increases, the solution becomes more viscous, and velocities of diffusion-controlled reactions, for example, disproportioning, slow down. It should be noted that special features of reduction of $AuCl_4^-$ and reactions of its disproportioning are intensely studied by many researchers [40–42]. As in the considered example, it is assumed that Au^{3+} transits to excited state, then reduces to Au^{2+}, which is unstable and disproportions with formation of Au^+ and Au^{3+}, then Au^+ reduces to Au^0 by other absorbed photon. The assumptions are made that nanoparticles can catalyze reactions of disproportioning [43].

Presence of UV or light radiation makes it possible to more flexible regulate characteristics of nanoparticles. For example, ammonium silver complex can be reduced by glucose at activation under light radiation at wavelength 365 nm at room temperature with stable dispersion of Ag nanoparticles with diameter 4–7 nm [44]. It is interesting to note that reduction of silver under the same conditions, but at heating and without UV impact, causes formation of nanoparticles with wide size distribution (4–100 nm). For the synthesis of anti-bacterial nanocomposite fibers, cellulose acetate (polyacrylonitrile, polyvinyl alcohol)/silver nanoparticles in DMF, which is simultaneously a solvent and a reduction agent, it is very efficient to apply UV radiation to increase yield of formed nanoparticles [45].

In the system of branched polyethyleneimine: 4-(2-hydroxoethyl)-1-piperazineethanesulfonic acid (HEPES): $AgNO_3$ photo-radiation causes oxidizing decomposition of polyethylene amine with following formation of positively charged Ag nanoparticles according to the proposed scheme (Scheme 3.2) [36]:

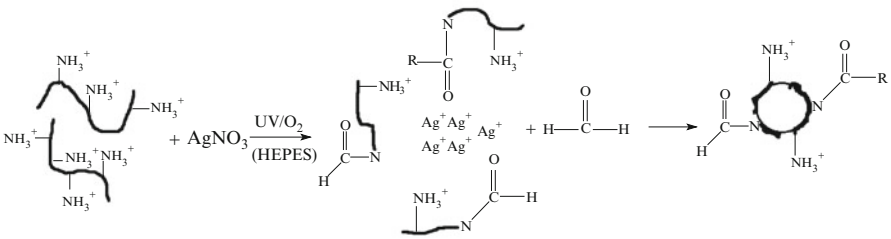

Scheme 3.2 The formation of branched PEI/Ag nanocomposite

It is assumed that formaldehyde formed as result of chemical transformation of PEI under UV treatment reduces silver ions, and HEPES has a catalytic effect on the process on the whole.

Important is the method of producing of nanocomposites, when polymerization and reduction processes induced by ultraviolet radiation are superimposed. Radicals formed under UV impact and being electron donors are able simultaneously polymerize monomers and reduce metal salts. Production of Ag nanoparticles and stabilizing polymer matrix is conducted in situ under irradiation ($\lambda = 320$ nm) of the mixture of monomer of 2-hydroxyethylmethacrylate and ammonium solution of silver oxide [46]. Often in these systems the main reactions are preceded by complex formation of metal ions with monomer molecules, as, for example, during formation of silver/polyacrylonitrile nanocomposite [47–49]. These processes can schematically be presented as:

$$Ag^+ + 2AN \rightleftharpoons \left[Ag(AN)_2\right]^+ \tag{3.9}$$

$$IN \xrightarrow{h\nu} IN^* \tag{3.10}$$

$$\left[Ag(AN)_2\right]^+ + NO_3^- \xrightarrow{h\nu} Ag^0 + 1/2O_2 + NO_2 + -(-AN-)_n- \tag{3.11}$$

$$IN^* + AN \rightarrow IN - AN^* \tag{3.12}$$

$$IN - AN^* + nAN \rightarrow IN - AN^* - (AN)_n \tag{3.13}$$

$$IN^* + Ag^+ \rightarrow IN^+ + Ag^0 \tag{3.14}$$

$$IN^+ + AN \rightarrow IN - AN^+ \tag{3.15}$$

$$IN - AN^+ + nAN \rightarrow IN - (AN)_n - AN^+ \tag{3.16}$$

where AN is an acrylonitrile molecule, IN is photoinitiator molecule.

The formed molecule of polyacrylonitrile plays a stabilizing role preventing aggregation of nanoparticles. The factors which allow control over nanoparticle sizes can be concentration of initial salt and content of a photoinitiator (Fig. 3.2).

Quite efficient control over nanoparticle size in such systems can be accomplished by usage of metal-containing monomers for precursors [50]. It can be demonstrated on the example of polystyrene/polyacrylic acid-Ag structured as polyelectrolyte brushes (see Sect. 2.2.3) [51]. Silver nanoparticles and polyacrylic chains are formed in situ during photopolymerization of silver acrylate on the surface of polystyrene particles coated by a thin layer of photoinitiator (2-[*p*-(2-hydroxy-2-methylpropiophenone)]-ethyleneglycol methacrylate) (HMEM) (Fig. 3.3). Radicals formed during UV irradiation initiate grafting polymerization of acrylate monomer and simultaneously reduce silver ions to metal Ag. Under these conditions local concentration of Ag^+ ions stays low, which causes expected ultrafine nanoparticle sizes (3 ± 1.2 nm).

Polyoxometalates of Keggin type (see Sect. 2.2.1) can serve as efficient matrix media for formation of metal nanoparticles due to their multielectron redox-chemistry and ability to accept and donor a certain number of electrons at some stages without decomposition [52, 53]. For example, under UV irradiation ($\lambda > 280$ nm) of the

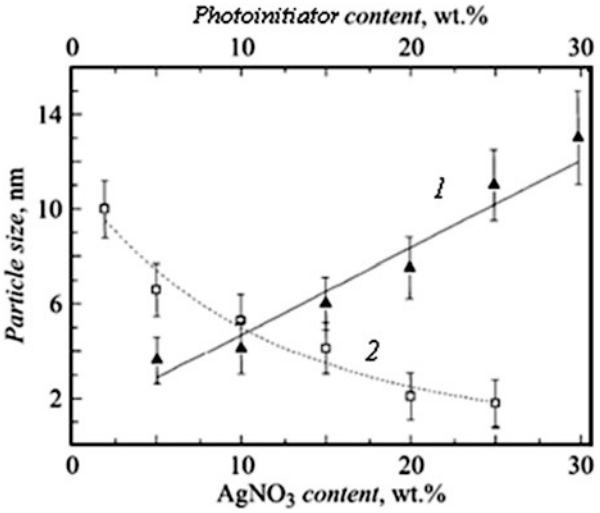

Fig. 3.2 Dependence of average grain size of silver nanoparticles on concentration of $AgNO_3$ (*1*) and photoinitiator (*2*) [47]

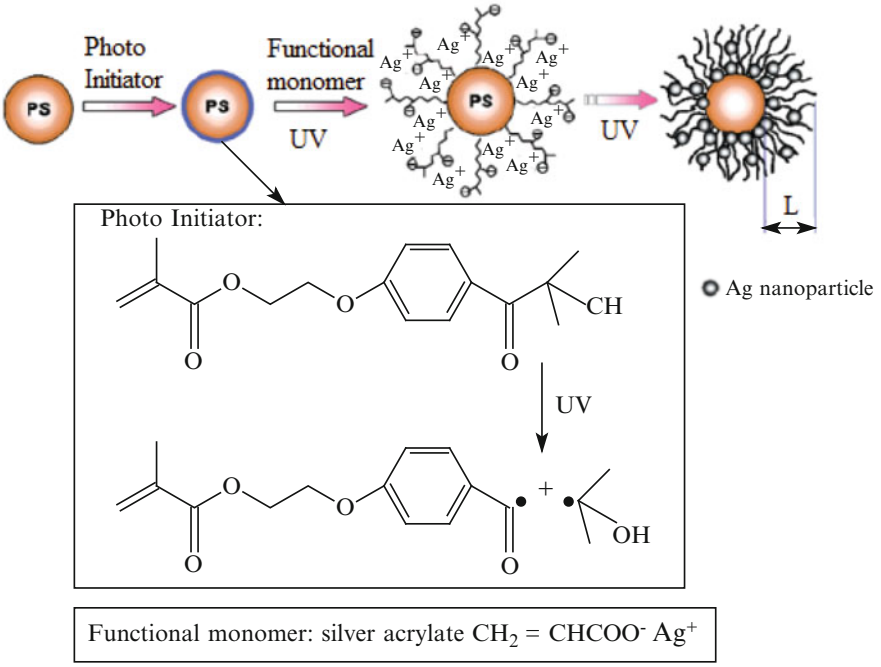

Fig. 3.3 Scheme of fabrication of PS-PAA-Ag composite particles *in situ* [51]

reaction mixture of $AgNO_3$ water solutions and $H_4(SiW_{12}O_{40})$ in presence of 2-propanol the following reactions take place [54]:

$$2(SiW_{12}O_{40})^{4-} + (CH_3)_2CHOH \rightarrow 2(SiW_{12}O_{40})^{5-} + (CH_3)_2C = O + 2H^+ \quad (3.17)$$

$$(SiW_{12}O_{40})^{5-} + Ag^+ \rightarrow (SiW_{12}O_{40})^{4-} + Ag \quad (3.18)$$

By the similar scheme photo-reduced interacts with $(SiW_{12}O_{40})^{5-}$ Pd^{2+}, $AuCl^{4-}$, and $PtCl_6^{2-}$ ions forming metal nanoparticles electrostatic and stoichiometric stabilized by Keggin ions [52]. In principle, the repeated irradiation can also reduce bound Keggin ions, and in this case polyoxometalates can be efficiently used for synthesis of bimetal nanoparticles as UV-switched reducing agents. This possibility is shown at production of Au-Ag nanoparticles with core-shell structure [53] in presence of phosphotungstic acid $H_3(PW_{12}O_{40})$ in propanol-2. Under irradiation by UV light (>280 nm, 450-W intermediate pressure lamp) single-electron reduction takes place during 4 h with formation of $(PW_{12}O_{40})^{3-}$ ions, which take immediate part in reduction of $HAuCl_4$ with formation of stable Au nanoparticles bound with Keggin ions. It is important that UV activation and reduction reaction of $AuCl_4^-$ do not touch the basic structure of the latter. Additional UV irradiation of Au-PTA solution brings to reduction of Keggin ions on the surface of nanoparticles and, in turn, addition of Ag_2SO_4 water solution completes by formation of Ag nanoparticles for 15 min. In the UV/visible spectrum of this solution there is weakening and blue shift of the plasmon resonance band of Au, while simultaneously appears a distinct absorption band at 415 nm, which confirms formation of Ag shell around Au core coated by PTA ions. The reducing agent bound this way and switched under irradiation provides reduction of the second metal just on the surface of the metal core, which makes this approach very promising in production of bimetallic structures, especially in catalysis.

It should be noted that thus obtained nanoparticles have long-term stability and, on the whole, the process is easily scaled.

3.2.2 *Photochemical Reduction in Solutions*

Photochemical reduction in the solutions is conducted in presence of electron-donor reagent and is most often used for synthesis of noble metal particles. Solutions of metal salts or their complexes in water, alcohol, and organic solvents are used as precursors and a medium for obtaining nanoparticles. In these media subjected to light exposure active particles form in form of solvated electrons:

$$H_2O \rightarrow aq\, e + H + OH, \quad (3.19)$$

or free radicals, to which, for example, belong ketyl, α-hydroxybenzene, benzoyl radicals, formed in reactions of photo-decomposition Norrish Type I [55, 56] of benzoin [57, 58], benzophenone [59–61] and other photoactivators. A typical representative widely used is 1-[4-(2-hydroxyethoxy)phenyl]-2-hydroxy-2-methyl-1-propan-1-on (Irgacure-2959,I-2959)[1]:

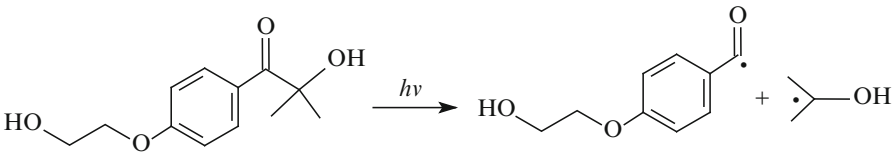

(3.20)

Active particles, in turn, via interaction with a metal ion, for example, Ag^+, reduce it to metal:

$$Ag^+ + aq\ e \rightarrow Ag^\circ \tag{3.21}$$

or

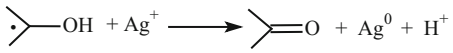

(3.22)

Three electron reduction of Au(III) ions can include several consequent stages of reduction and disproportioning [63, 64].

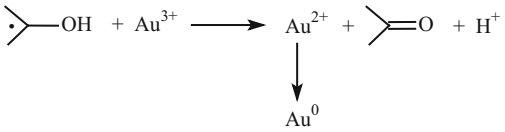

(3.23)

Efficiency of the photo process is such that under exposure of UV light >320 nm gold nanoparticles form during several minutes [64]. Redox potentials of ketyl radicals make all stages of reduction of Au^{3+} ions thermodynamically preferable [42].

[1] Irgacure-2959 has sufficient solubility in solvents with different polarities, such as water, toluene, THF, etc. Quantum yield of its photodecomposition is 0.29 and the processes of extinguishing of triplet state by ion metals almost do not go since times are short, which, on the whole, provides high efficiency of reduction reactions [62].

Photoinitiator 1-hydroxycyclohexylphenyl ketone forms two free radicals during photolysis:

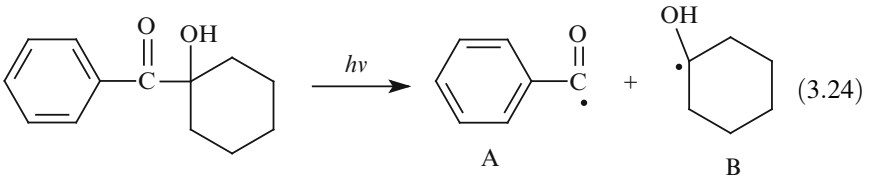

(3.24)

Chromatography and mass-spectral analysis were used to identify products of photolysis during the reduction reaction of coordination compound $CuCl_2$ with diethanolamine in the ethanol medium [65] and main ways of photochemical transformations in the system are found. Free radical A can split a hydrogen atom from ethanol molecule or from free radical B with formation of benzaldehyde (Scheme 3.3). In the other way A and B can recombine the initial photoinitiator, or two free A radicals interacting with each other form a couple:

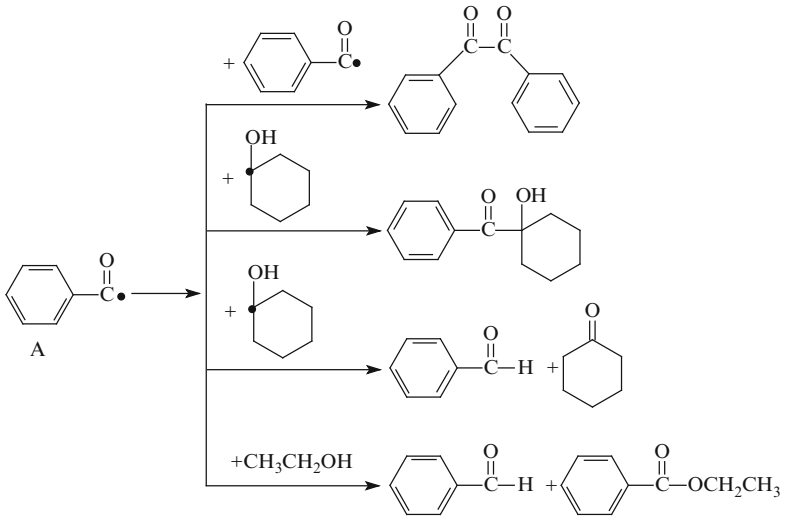

Scheme 3.3 The routes of a primary radical transformation at photoreduction of $CuCl_2$ in the diethanolamine-ethanol system

In no one of these transformations free radical A loses electrons, which points to the fact that it does not take part in reduction of copper ions. But, taking into account that in other products of the photochemical reaction cyclohexanol and cyclohexanone are found, corresponding to B radical by their chemical structure,

probably, the main channels of the reduction reaction of copper ions proceed with participation of B radical, as is shown in the following scheme (Scheme 3.4):

Scheme 3.4 The routes of the $CuCl_2$ transformations in the diethanolamine-ethanol system

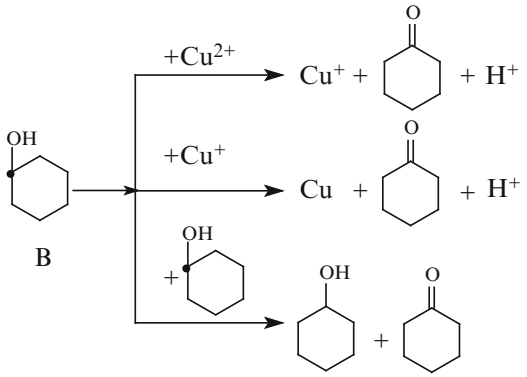

Color molecules can play a double role as photosensitizers: they can initiate protecting function for nanoparticles and modify their optical properties. Experimental data [35] confirm that, for example, thionine molecule

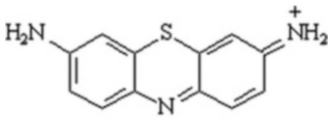

Thionine (TH^+)

under action of light transforms into singlet and triplet states:

$$TH^+ + h\nu \rightarrow {}^1TH^+ \rightarrow {}^3TH^+ \tag{3.25}$$

The formed triplet in absence of donors or acceptors of electrons can take part in disproportioning reaction with a non-excited thionine molecule with formation of oxidized and reduced products with electron transfer in non-polar medium at the rate 7.3 $(\pm 0.3)\cdot 10^7$ M^{-1} s^{-1}:

$${}^3TH^+ + TH^+ \rightarrow TH^\bullet + TH^{\bullet 2+} \tag{3.26}$$

$$TH^\bullet + Ag^+ \rightarrow TH^+ + Ag^0 \tag{3.27}$$

Rate of the direct reaction of extinguishing of triplet state by silver ions is small $(1.30\ (\pm 0.06)\cdot 10^6$ M^{-1} $s^{-1})$, which makes this reaction of electron transfer with formation of metal nanoparticles barely probable, as was discussed above. It should be noted that realization of photosensitized reduction of metal ions in water medium is possible only at participation of electron donors, for example, triethanolamine.

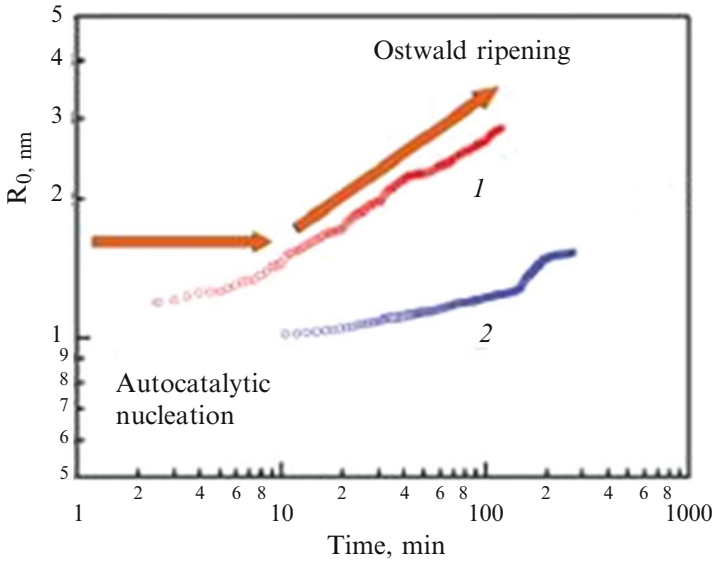

Fig. 3.4 Average radius (R_0) as a function of the reduction time for the metallic Pd (*1*) nd Rh (*2*) nanoparticles produced during the photoirradiation [67]

SAXS measurements in situ with time resolution made it possible not only to find mechanism of formation of Ag [66], Rh and Pd [67, 68] nanoparticles at photoreduction in the system of ionic precursors and surfactant of poly(N-vinyl-2-pyrrolidone), which includes consequent conjugate stages of autocatalytic reduction, nucleation, nucleation-growth, Ostwald ripening and dynamic coalescence, but also compare rates of individual reactions. Typically, depending on a kind of metal and its concentration, prevailing processes can be autocatalytic reduction-nucleation with the following growing stage in combination with coalescence, as in the case of Rh nanoparticles, or rapid reduction-nucleation with high velocities at the early stage and, then, via Ostwald ripening, to diffusion-limited growth of nanoparticles, as in the case of Pd (Fig. 3.4).

It should be noted that metal nanoparticles, especially noble, are very photoactive and under action of UV irradiation strongly polarized. This brings to positive charge of metal aggregates consisting of small clusters and, as a consequence, to their instability and decomposition by components [69, 70]. Since free metal ions present in a solution in substantial concentrations, at the initial state this causes formation of a great amount of small clusters, which rapidly coagulate in great aggregates. Nuclei with less than critical size are dissolved due to thermodynamic instability and provide growth of coarser particles. In turn, coarser aggregates are photo-chemically unstable and decompose under UV irradiation. On the whole, mechanism of formation of nanoparticles under UV irradiation can be considered as quasi-equilibrium [71], accompanied in parallel by growth and

fragmentation processes, which in turn causes thermodynamically stable particles with relatively narrow size distribution.

Efficiency of photo-chemical synthesis of metal nanoparticles can, in the first place, decrease due to intense extinguishing of excited state of photoinitiator or photosensitizer by metal ions which are precursors of nanoparticles [64]. Thus, Ag (I) ions can suppress excited states of carbonyl compounds with the rate constants close to the values typical for diffusion-limited reactions [72]. In principle, these problems can be avoided if systems are used in which photo-induced processes required for metal ion reduction can be separated in time or space. For example, strategy of efficient photochemical synthesis, not only for Au nanoparticles, but with regard to other metals, can be put down to two main approaches proposed in [55]. This is, first of all, achieved by usage of monomolecular precursors (for example, benzoin derivatives such as already mentioned I-2559) with short lifetime of triplet state (10 ns or less) and effective absorption in UV region (315–400 nm). Another approach is in spatial segregation of radical-generated reaction from the stage of electron transport, which causes reduction of metal ion. To do this, one can use numerous self-assembling systems, for example, micelles such as sodium dodecyl sulfate, etc. The main demand to them is transparency in the region of UV absorption and absence of structural groups capable of barren extinguishing of triplet state.

Yield of ketyl radicals increases significantly at addition to the system of effective hydrogen donor. In [55] for this purpose 1,4-cyclohexadiene was used, its hydrophobic character is especially favorable for micellar systems. The process with participation of cyclohexadiene is illustrated by the following scheme (Scheme 3.5).

Scheme 3.5
Transformations of ketyl radicals in the presence of 1,4-cyclohexadiene

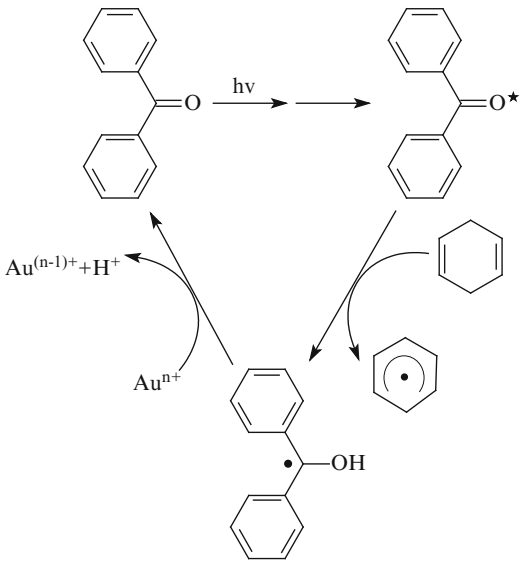

Cyclohexadiene radical is also a good reducing agent and can contribute to reduction of metal ions.

3.2.3 Photo Reduction on Solid Substrates

Chemical interaction of a solid substance with electromagnetic irradiation goes not only on a surface, but in surface layers of about several microns. Formation of nanoparticles in radiation stimulated solid phase processes is predominantly caused by reactions of photochemical decomposition. As regards other mechanisms, the considered method can have some limitations, because not all used matrices can be photochemically active, i.e. able to generate free electrons in the system under action of UV light, as it is typical, for example, for TiO_2. The TiO_2 gel films have intense absorption in the range of 250 nm, and under exposure at 254-nm irradiation, couples form: hole-free electron. This approach is successfully used for fabrication of Pt nanoparticles encapsulated in microporous carbon hollow shell [73]. For precursor the Pt(IV) compound and phenol served absorbed on the surface of titanium oxide powder. Photo generated electrons of metal oxide matrix causes reduction of Pt(IV) and oxidization of phenol with formation of phenol polymer on the surface of TiO_2 particles with Pt (~3 nm) particles encapsulated in organic matrix. The following carbonizing at 700 °C and removal of TiO_2 by dissolution causes formation of hollow carbon spheres with 3–5-nm thickness with incorporated metal particles. It is interesting that formed nanocomposites show effective catalytic properties in hydration of cyclohexene with higher TOFs (turnover frequencies), than for a catalyst obtained by impregnation.

Combination of photo irradiation with ultrasonic treatment causes penetration of metal salt into pores of a carrier and deposition of metal nanoparticles not only on surface, but also in inner pores of TiO_2 matrix [74].

On the whole, the process of photochemical deposition of nanoparticles can be implemented in two ways. In the first way, matrix on a solid substrate is immersed in a solution of a metal precursor, and this system is irradiated. In the second way first the solution of metal salt is subjected to photolysis, and then a substrate, for instance, film, is immersed in it. These procedures of reduction were used for plating of TiO_2 surface or indium-tin oxidized film (ITO) by Pt, Au or Ag nanoparticles [70]. A number of particles of deposited metal is regulated either by concentration of a metal salt and/or by holding time of a film in irradiated solution. It should be noted that nanocomposite materials of this type can be used as photo catalytic films in devices with self-cleaning surfaces or for water and air purification from contaminants [75, 76], and also as new electrode materials in electrochemistry [70].

Polysilanes are known as photosensible materials [77], UV irradiation causes break of Si-Si bond due to formation of silyl radicals, which can play a role of reducing agent [78]. Metal nanoparticles are formed on a surface of polystyrene

particles containing incorporated molecules of poly(methylphenylsilane) (PMPS) by the following scheme (Scheme 3.6) [79]:

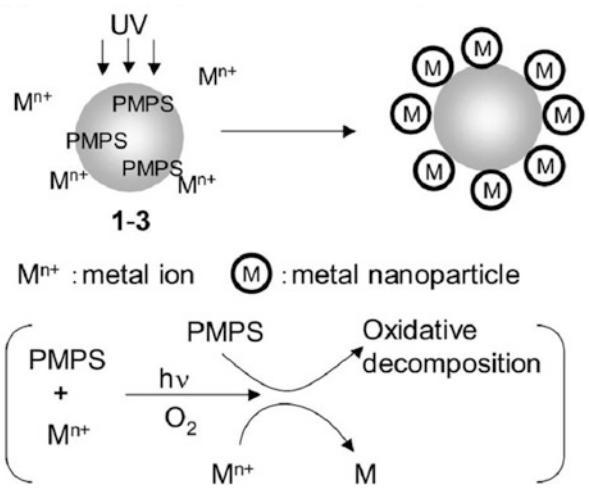

Scheme 3.6 Reduction of metal ions with the participation of polymethylphenylsilanes on the surface of polystyrene

Under action of UV radiation photo oxidized decomposition of PMPS proceeds, which is accompanied by reduction of metal ion.

For carries used for immobilizing of metal ions most often are used polymers [80–82] or inorganic matrices such as TiO_2 [83–85], SiO_2 [86, 87]. Film nanocomposites can be fabricated in two ways. One of them provides films of 20–200 μm thickness by pouring and centrifuging from a polymer solution containing a metal precursor compound [81], after UV irradiation heating to various temperatures can be applied, which do not exceed glass transition temperature of a polymer. Silver nanoparticles in a matrix of linked oligourethane methacrylates are synthesized by impregnation of polymer plates with 2,2-dimethyl-6,6,7,7,8,8,8-heptafluoro-3,5-octanedione Ag metal organic complex in the medium of supercritical CO_2 [82] and the following radiation by filtrated radiation at $\lambda = 365$ nm from a mercury lamp. The size distribution function for nanoparticles and their concentration are controlled by different factors, such as structure of a matrix of impregnated polymer, type of solvent, temperature and other conditions of impregnation. It is interesting that this approach makes a possibility for designing in polymer matrices various optical microstructures consisting of nanoparticles, which would have varying refraction and absorption coefficients. In the other way metal containing precursor can be introduced in the initial polymer system, however, in this way the process is often complicated by interaction reactions of a metal compound with monomer or initiator molecules, inhibiting of polymerization reactions, etc. Only specially found conditions by type and concentration of the initial state of a metal, type of initiator, and

temperature of reaction are suitable for production of nanocomposites, for example, as in MMA system and tetrachloroaurate (III) N-cetylpyridinium (Scheme 3.7) [88]:

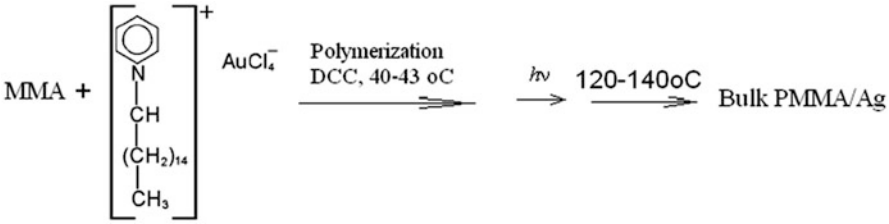

Scheme 3.7 Synthesis of a nanocomposite by polymerization in situ followed with photoreduction. *DCC* dicyclohexyl peroxydicarbonate

Character of interaction between metal ions and functional groups on a surface of polymer particles has a substantial effect on formation and immobilizing of metal nanoparticle. Opposite results were obtained in the polystyrene/PMPS and $HAuCl_4$ $4H_2O$, $AgNO_3$, Na_2PdCl_4 salts system depending on a type of surface carrier (cation or anion) and type of functional group of polymer particle (Table 3.6) [79].

As is seen from Table 3.6, interaction between cation polymer particle and metal ion (Ag^+, Pd^{2+}) impedes formation of metal nanoparticle on a surface of the polymer particle, while interaction between anion polymer particle and anion complex ion $AuCl^{4-}$, $PdCl_4^{2-}$ has no such effect and brings to formation of nanoparticle/polymer

Table 3.6 Preparation of Metal Nanoparticle/Polymer Hybrid Particles [79].

Polystyrene particles (surface charge and coordinative group[a])	Metal salt	Metal particles on the polymer surface	
		Morphology	Size, nm
PS (anionic)	$HAuCl_4 \cdot H_2O$	Sphere	10–20
PS (cationic)	$HAuCl_4 \cdot H_2O$	Sphere	10–20
PS-co-NIPAM (90:10) (anionic, NIPA)	$HAuCl_4 \cdot H_2O$	Sphere	10–20
PS-co-NIPAM (90:10) (cationic, NIPA)	$HAuCl_4 \cdot H_2O$	Sphere	10–20
PS (anionic)	$AgNO_3$	Sphere	10–20
PS (cationic)	$AgNO_3$	[b]	
PS (anionic)	Na_2PdCl_4	Sphere	<10
PS (cationic)	Na_2PdCl_4	Sphere	<10
PS-co-NIPAM (90:10) (anionic, NIPA)	Na_2PdCl_4	Shapeless	>10
PS-co-NIPAM (90:10) (cationic, NIPA)	Na_2PdCl_4	Sphere	<10
Poly(St-co AAEM) (99:1) (anionic, AcAc)	Na_2PdCl_4	Shapeless	>10
Poly(St-co AAEM) (99:1) (cationic, AcAc)	Na_2PdCl_4	Sphere	<10
PS-co-NIPAM (90:10) (anionic, NIPA)	$PdCl_2$	Shapeless	>10
PS-co-NIPAM (90:10) (cationic, NIPA)	$PdCl_2$	[b]	

[a]*NIPA* is N-isopropylacrylamide group; *AcAc* is acetoacetoxy group
[b]Metal particles were not formed

hybrid composite. The mechanism of photoreduction of silver on SiO_2 is supposed [89] which includes the donation of electron from silica to silver ions fixed on the oxide surface under UV irradiation. It is shown [90] that there are many differences in formation of Ag nanoparticles depending on whether there is reduction of free Ag^+ ions or ions absorbed on a surface of colloid silica gel. In presence of oxide carrier formation and aggregation of nanoparticles was predominantly on its surface due to absorption of Ag^+ ions on negatively charged surface of silica gel. Probably, here SiO_2 surface plays a double role: attracts and bonds positive silver ions, and also under irradiation supplies by electrons, which reduce metal ions.

By changing size of the surface of colloid silica gel ($S_{spec} = 140–345\ cm^2/g$), density of silver nanoparticles on silica gel particle can be controlled.

On the whole, photochemical deposition of metal nanoparticles minimizes usage of chemical reagents, solvents, and, consequently, is ecologically more attractive than chemical ways considered above. However, problems of control over nanoparticle size and their distribution on a solid substrate in many cases are not solved. It is significant, for example, that hybrid nanocomposites based on noble metals (Ag, Au, Pd, Pt) obtained in thin TiO_2 films by the following Scheme 3.8 [91] have

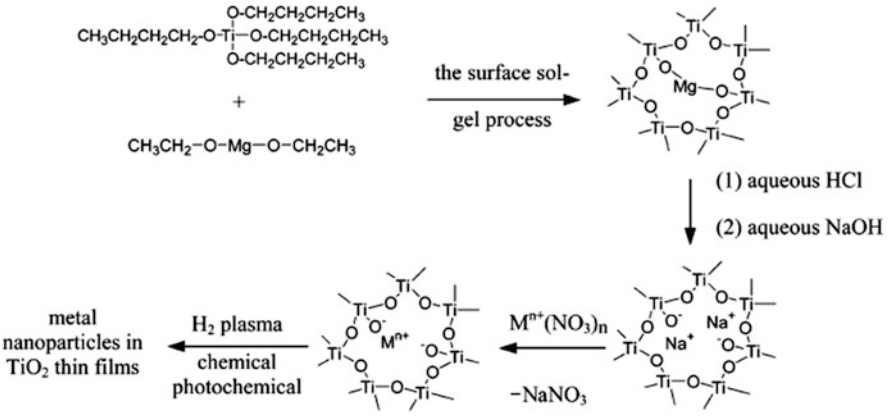

Scheme 3.8 Hybrid nanocomposites in TiO_2 thin films

different sizes of nanoparticles depending on reduction method. Average diameter of Ag nanoparticles and standard deviation (dispersion) are 6.0 ± 1.8 nm at usage of $NaBH_4$, 8.6 ± 3.0 nm at reduction by H_2 plasma and 7.6 ± 3.0 nm under UV irradiation.

3.2.4 Photo Induced Processes in Nanoparticles

Apart from photo reducing reactions, which have as a result formation of nanoparticles under light of UV irradiation the formed nanoparticles can be

subjected to structural or morphological changes due to their high photochemical activity. Two main effects can be shown. On the one hand, individual particles or their aggregates can be subjected to photo fragmentation [70, 71, 92]. This mechanism can be caused by photo induced generation of electrons in a nanoparticle, which are injected in environment, consequently nanoparticles accept positive charge. Electron ejection brings, in turn, to destabilization of a nanoparticle or a nanoaggregate with the following fragmentation and formation of metal clusters. On the other hand, UV and light excitation can cause photo induced increase in temperature of a nanoparticle, which promotes partial melting of aggregates [93], accompanied by coalescence of neighbor particles, and, as a result, by formation of coarser individual nanoparticles. In accordance with these mechanisms, disappearance of Pt nanoparticles with 20 nm sizes and appearance of particles in H_2PtCl_6/TiO_2 system is, probably, caused by photo induced fragmentation of initially formed polycrystalline aggregates under UV exposure for 15 h [70]. Similar processes are described for gold and silver nanoparticles [92, 94]. Photochemical activity of metal nanoparticles promotes photo induced generation of charges and the following formation of charged metal particles. In turn, electrostatic repulsion forces raised between these particles can stop particle growth after quite long exposure to UV radiation. In these systems it is possible to obtain stable suspensions of nanoparticles for their long-time storage as it has been shown for Au particles [70]. No changes were observed in UV-visible spectrum range after 2 weeks of storage of $HAuCl_4$ solution subjected to photolysis during 3 h (Fig. 3.5).

As is seen, the band at 225 nm corresponding to charge carrier metal-ligand for the initial chloraurate complex significantly decreases in the first minutes of UV

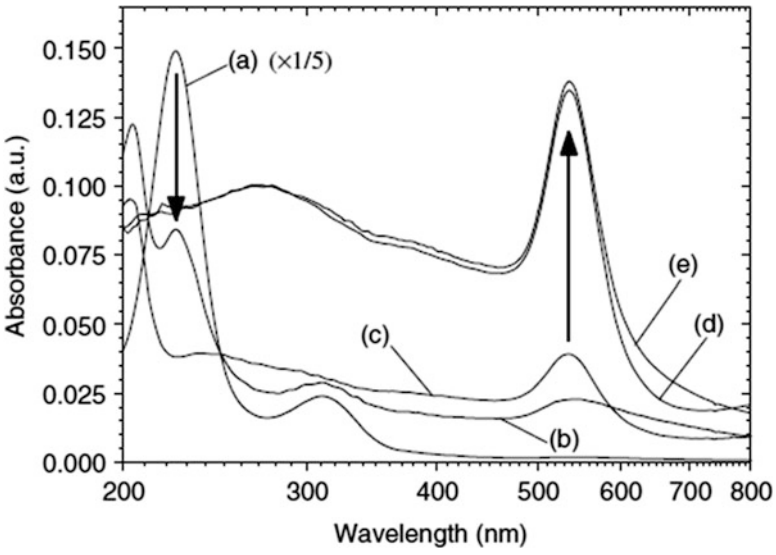

Fig. 3.5 UV-visible spectra of a 250-mM $HAuCl_4$ solution exposed to UV light for 0 (*a*), 2.5 (*b*), 45 (*c*) and 180 min, before (*d*) and after ageing in ambient conditions for 2 weeks (*e*) [70]

exposure, which points to photolytic reduction of salt. Simultaneous appearance of a band at 205 nm is, probably, caused by previously considered consequent reduction from Au^{3+} to Au^{1+} and further on to Au^{0}.

Thus, action of light produces photo effect, which can substantially change properties of immediate surrounding of metal nanoparticles. Respectively, this causes instability of colloid, for example, eliminates stabilizing impact of polymer shell, induces changes in size and shape of nanoparticles, and initiates their clustering, i.e. formation of aggregates consisting of hundreds to thousands superfine metal nanoparticles. Generation of particles with different shape and sizes and a change in distance s between particles in aggregates is expressed in appearance of additional absorption peaks and inhomogeneous broadening of resonance absorption peak. It has been found [95] that as after irradiation by mercury lamp plasmon resonance band of Au at 532 nm broadens and disappears, and a band appears at 840 nm, which is related to dipole-dipole interaction of particles in aggregates. It is found that aggregation rate depends on a solvent type and light wavelength. The effect of light wavelength is caused by increase in Van-der-Waals forces and by a change in Coulomb interaction of surface charges. Exchange by electric charges generated due to photoemission is caused by a dependence of Fermi energy on particle size, passes through dispersion medium and brings to equalization of potential of particles of different sizes. As a result of exchange, long-range electric forces appear, which promote approach of the particles to distances corresponding to Van-der-Waals forces, which cause aggregation.

Distances between particles are in inverse relation to usually observed spectral shift [96]. While polychrome light can increase aggregation rate [97, 98], laser impact is accompanied by photo modification of the aggregates [99]. As a rule, aggregation rate and properties of the formed aggregates depend on method of synthesis of nanoparticles. Coarse aggregates usually have loose dendrite-like structure with fractal properties.

Irradiation of colloid silver obtained by citrate method in the $AgNO_3/NaBH_4$/sodium citrate/bis(p-sulfonatophenyl) phenylphosphine dihydrate dipotassium system by fluorescent lamp (7 mW/cm^2) during 20 h is accompanied by significant modification in shape of nanoparticles and formation of nanoprisms [100]. At the same time, usage of laser on argon ions ($\lambda = 514.5$ nm) in the colloid system based on $AgNO_3$/ethanol/poly(vinylpyrrolidone) (PVP) is efficient for structuring of large aggregates with the structure of statistical fractals with ~5,000 nm length.

3.3 Radiation-Chemical Reduction

In radiation-chemical reduction usually γ-radiation is used (for example, on ^{60}Co sources). Radiolysis is conducted in stationary conditions (constant radiation flow) or in alternate conditions (intermittent flow with pauses or pulse, when once for a short time high doze is applied) [101]. Radiation-chemical yield for each system depends on a great number of physical and chemical factors (time and absorbed

energy, concentration of reacting substances, temperature, mass transport, pH of a medium, etc.), which change during irradiation. In a common case radiation yield being a number of active particles (molecules, ions, radicals, etc.) per 100 eV of absorbed energy is a function of absorbed radiation doze. Initial yield of intermediate products of radiolysis (electrons, ions, excited particles) is a value of about 10. Observed values of radiation yields are in wide range from 10^{-6} to 10^{8} particles per 100 eV [102]. Thus, for active particles which generate during radiolysis of water, the highest yield is typical of hydrated electrons e^{-}_{aq} (2.6), OH^{-} (2.7), H^{+} (2.6), for H, H_2 and H_2O_2 it is 0.6, 0.45 and 0.7, respectively [103]. The formed e^{-}_{aq} and hydrogen atom have high reduction potentials (−2.9 and −2.3 V, respectively), which allows, for example, in to reduce Cu^{2+} ions in triple polyelectrolyte PAA-PEI- Cu^{2+} complex to metal copper Cu^{0}, while in this system Cu_2O-based nanocomposite is obtained in presence of strong chemical reducing agent [104].

Oppositely, hydroxyl radical has high oxidizing ability (1.9 V). In order to avoid side reactions with participation of OH^{-} radicals, such as oxidation of metal ions, linking reactions, and destruction of macromolecules, organic substances are added to the system, for this purpose alcohols and salts of organic acids are used. In the case, for example, of isopropyl alcohol or formate-ions, as a result of reactions

$$(CH_3)_2CHOH + OH\,(H) \rightarrow (CH_3)_2COH + H_2O\,(H_2) \tag{3.28}$$

$$HCOO^{-} + OH\,(H) \rightarrow CO_2^{-} + H_2O\,(H_2), \tag{3.29}$$

initiated by impact of ionizing radiation on water solution, only reducing particles form in it, in particular $(CH_3)_2COH$ or CO_2^{-}, whose reduction potentials are −1.4 and −1.9 V [103].

Radiolysis in condensed matter is conventionally divided in three stages [102]. The first, physical stage is associated with formation of primary intermediate products and is rather fast (less than $3 \cdot 10^{-16}$ s). Second, physical-chemical stage is associated with spatial distribution of primary intermediate products and homogenization of a system as a result of transport process (for example, diffusion). In liquids with medium viscosity it is completed for 10^{-8}–10^{-7} s. During radiolysis, in contrast to photolysis, distribution of obtained intermediate particles is more homogeneous and provides synthesis of narrowly distributed particle sizes. The third, chemical stage includes processes of chemical transformation in volume of homogenized system. Duration of this stage is determined by average time of chemical transformation and can be infinitely long. In gas phase the second stage usually does not manifest itself due to high diffusion rate of primary products of radiolysis. On the contrary, in solids (especially at low temperatures), where diffusion rate is low, radiolysis can delay at the second stage.

3.3.1 *Kinetics and Mechanism of Radiation-Induced Synthesis of Nanocomposites*

Usage of pulse γ-radiolysis in combination with spectrophotometry made it possible to study experimentally on example of reduction of silver [103, 105], gold [103, 106], and copper ions [107] mechanism and kinetics of initial stages of formation of metal colloids in water, water-alcohol, and non-water solutions, whose basic principles have, probably, general character. One of advantages of radiolytic method is homogeneous and instant generation of a great number of atoms during irradiation, which provides favorable conditions for formation of monodisperse particles.

At early stages of transformation after fast one-electron reduction of metal ions follows disproportioning with formation of simple atomic and ionic clusters (Ag_2^+, Ag_2, Ag_4^{2+}, Ag_4^+, etc.), or clusters and intermediates (in the case of formation of copper colloids in presence of formate ions, $CuCO_2$, Cu^+, Cu^{2+}). Interaction of these associates causes formation of subcolloid particles containing one-two tens atoms (for example, 8–16 Ag atoms with maximum absorption at 325 nm [108, 109], 10 Pd atoms with maximum absorption at 320 nm) [103]. These processes proceed for times no less than 1 s after γ-pulse. In some cases subcolloid forms (for example, clusters Ag [110], Pd [111]) can be stable during several days.

Mechanism of transformation of reduced metal ions to nanoparticles on the example of formation of subcolloid particles [112] can be presented by the following scheme (Scheme 3.9):

$$Cu^{2+} \xrightarrow{CO_2^-,\ e_{aq}^-} CuCO_2 \xrightarrow{Cu^{2+}} Cu_2^+ \xrightarrow{x\ Cu_2^+} Cu_j^{m+} \longrightarrow Cu_n^0$$

Scheme 3.9 Formation of subcolloid Cu particles

or in general form (Scheme 3.10):

Scheme 3.10 The main steps of the formation of colloidal particles

Active species generation:

$$H_2O \xrightarrow{h\nu} H^\bullet,\ OH^\bullet,\ e_s^-,\ H_3O^+,\ H_2,\ H_2O_2$$

$$OH^\bullet(H^\bullet) + RH \longrightarrow R^\bullet + H_2O\ (H_2)$$

Metal reduction:

$$M^{n+} + nR^\bullet \longrightarrow M^0 + nR^\bullet + nH^+$$

$$M^{n+} + ne_s^- \longrightarrow M^0$$

Growth of colloids:

$$nM^0 \longrightarrow M^0_{colloid}$$

Formation of metal colloid during γ-radiolysis is accompanied by narrow plasmon band in absorption spectrum, which is typical of spherical particles with similar size distribution and weak interaction with a solvent. Changes in electron

state from clusters with atomic-molecular characteristics to nanoparticles are well tracked in optical spectra. Individual narrow optical bands typical of clusters of different complexity, as cluster grows, transform into wide optical bands typical of quasi-metal particles, and then into plasmon absorption band, corresponding to metal state. The $Au_{18}Ag_{20}$ и Au_{55} particles show obvious surface plasmon resonance, whereas for clusters consisting of 8–13 atoms atomic-molecular electron state is typical [103]. Properties of intermediate sized particles are approximately quasi-metallic and, probably, they serve nuclei of metal phase and have tendency to growth. Presence of indifferent electrolyte $NaClO_4$, and OH^-, SO_4^{2-}, $HCOO^-$ ions, which are prone to specific sorption on a metal, accelerates nucleation process of silver or other metal.

Unusual reduction kinetics is shown by cobalt and nickel ions under γ-irradiation of de-aerated $2{\cdot}10^{-5}$–$5{\cdot}10^{-2}$ *M* solutions of $Co(ClO_4)_2$ and $Ni(ClO_4)_2$, containing HCOONa. Formation of metal is preceded by induction period (Fig. 3.6) and reduction is developed in autocatalytic regime, formation of metal soles and increase in their concentration accelerates the process.

These behavior of reduction of metal ions is explained by the ratio of reduction potentials of their intermediate oxidized forms and redox potentials of formed organic radicals $(CH_3)_2COH$ in the system with isopropyl alcohol and CO_2^- in presence of formate ions. Potentials of E^0 $Ni^{2+}/Ni^0 = -2.2$ V and $Co^{2+}/Co^0 = -2.33$ V pairs are more negative than for massive metals, and $E^0(Co^{2+}/Co^+)$ and E^0 (Co^+/Co^0) are −1.8 V and −2.9 V, respectively. Since that, hydrated electron (−2.9 V) can

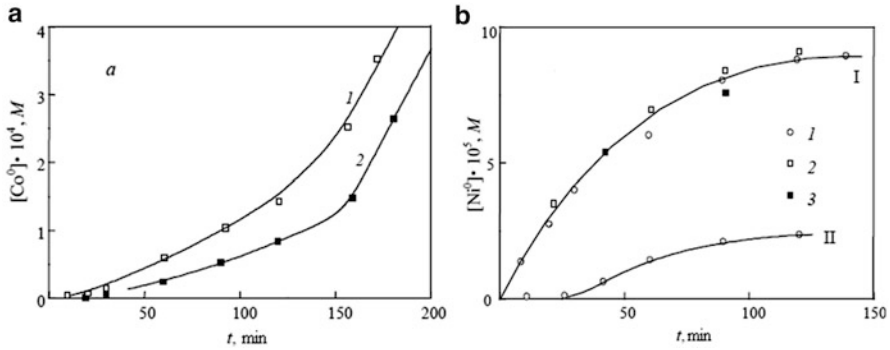

Fig. 3.6 Concentration of colloidal cobalt (**a**) and nickel (**b**) in the reaction solution as a function of the γ-irradiation time. (a) Solutions of $Co(ClO_4)_2$ with concentrations of $5{\cdot}10^{-3}$ *M* (*1*) and $1{\cdot}10^{-3}$ *M* (*2*); the admixtures are HCOONa (1×10^{-2} *M*) and polyacrylate (1×10^{-3} *M*). *Radiation dose* rate is 1 kGry/h, for 1 min of irradiation $4{,}4{\cdot}10^{-6}$ *M* e^-_{aq} and 5.6×10^{-6} *M* CO_2^- are formed. (b) Solutions of $Ni(ClO_4)_2$ with concentration of 1×10^{-4} *M*; the admixtures are polyethylene imine (*1*), polyacrylate (*2*), polyvinyl alcohol (*3*), HCOONa (I) or isopropyl alcohol (II). *Radiation dose* rate is 0. kGry/h, for 1 min of irradiation 2.2×10^{-6} *M* e^-_{aq} and 2.8×10^{-6} *M* CO_2^- are formed [103]

efficiently reduce Co^{2+} ion. Method of pulse radiolysis has confirmed the reaction realization ($k = 1.1 \cdot 10^{10}$ l·mol^{-1}·s^{-1}) (ref. by [103]):

$$Co^{2+} + e^-_{aq} \rightarrow Co^{+} \tag{3.30}$$

3.3.2 *Fabrication of Polymer Nanocomposites* In Situ

Initial stages of radiation-chemical reduction of metal ions should conduct under anaerobic conditions. To obtain stable nanoparticles and prevent coalescence of atoms, radiation reduction is performed in presence of stabilizing agents, among which most often are used various polymers such as polyethylene amine, polyvinyl sulfate [103], polyvinyl alcohol [113], poly(*N*-vinylcarbazole) [114], polyacrylonitrile [115], dendrimers, etc. Functional groups of polymers with high affinity to metal provide fixation of a molecule on a particle surface, and polymer chains in parallel to such factors as electrostatic repulsion and steric obstacles prevent particles from sticking to each other.

The considered method of producing of nanocomposites in situ includes solution, and often, a complex formation of metal salt with a polymer in water, water-alcohol, and non-polar media and the following reduction of metal ion under γ-irradiation. There are interesting approaches when the processes of formation of a nanoparticle and polymer matrix are joined. Gamma-induced polymerization of *N*- vinylcarbazole, particularly, its co-polymerization, since acrylic acid was added to the system, and formation of silver nanoparticles, cadmium sulfide and hetero-metal nanoparticles of Pd_{50}–Ag_{50} and Pt_{50}–Ru_{50} alloys (considered below) occurred simultaneously under action of γ-irradiation of 30 kGy at the doze power 1.0×10^4 Gy/h [114]. The same method was used to fabricate Ag/poly aniline nanocomposites with core-shell structure. Water solution of aniline, free radical initiator and silver salt were irradiated by γ-rays [116]. Reduction of silver salt in water aniline brings to formation of Ag nanoparticles, which in turn, catalyze oxidation of aniline to polyaniline.

Variation of in situ is fabrication of hydrogel nanocomposites, which are obtained by preliminary linking of polymer gel by gamma-radiation, then swelling of the linked polymer with metal salt and alcohol (isopropyl) water solution, and following by metal ion reduction. Silver nanocomposites stabilized in matrices polyvinyl alcohol/cellulose acetate/gelatin [117] and polyvinylpyrrolidone/alginate [118] were synthesized with usage of γ-radiation of no less than 25–40 kGy doze. Functional groups of the polymer system such as –OH, C = O and –NH work as templates for binding metal ion and provide homogeneous distribution of formed nanoparticles in hydrogel matrix. Additional advantages of the radiolysis here are in a possible combination in one process of polymerization, linking, and sterilization of hydrogel (the latter is important, for example, for using of such composites as dressing for wounds[2]) due to the fact that primary OH

[2] Doze 10 kGy provides sufficient sterilization of these materials [119].

Table 3.7 Mechanical properties, surface area and mean pore diameter of diisocyanate cross-linked silica aerogel composites

Metal loading	Density, g/cm^3	Load at fracture, kg	Elasticity modulus, MPa	Specific surface, m^2/g	Average pore diameter, nm
Au	0.56	19.15	77.35	164	19.6
Ag	0.58	16.07	62.80	164	19.6
Without metal	0.57	14.7	67	150	19.4

Diisocyanate concentration in the bathing solution before curing was 50 % w/w. Metal concentration was 3×10^{-4} mol $\cdot$ L^{-1} in both cases. Metal-loaded samples were irradiated with a total dose of 7 kGy. The plain sample was non-irradiated. Typical inaccuracy of the experimental data is $\pm$10 % [123]

radicals interacting with hydrogel molecule generate polymer radicals, which participate in linking of chains. A degree of linking is well controlled by doze of radiation irradiation.

As in other methods of reduction, multi parametric control may be performed over dispersion and shape of particles. Average diameter of Ag nanoparticles and their distribution increased as a precursor concentration increased. Impregnation of hydrogel system: polyvinyl alcohol/cellulose acetate/gelatin with $AgNO_3$ with concentrations 5.10 and 20 mmol brought to formation of nanoparticles with average diameters 38.6, 56.8, and 60 nm, respectively [117].

In order to obtain mechanically strong hydrogel nanocomposites, approaches are developed for encapsulation of metal nanoparticles in aerogels with high strength characteristics [120–122]. In particular, silica gel hydrogels were produced by reactions of based-catalyzed catalysis and linking with di-isocyanate [123]. The linked hydrogel is multiply rinsed (by 12 h each time) by metal salt solution and bombarded by gamma-radiation. It should be noted that incorporation of metal nanoparticles and used irradiation doses do not have undesirable effect on mechanical properties and chemical composition of composite aerogel (Table 3.7).

3.3.3 γ – Radiolysis in Synthesis of Semiconductor Nanomaterials

Radiation-chemical method is one of the most efficient methods of producing of metal chalcogenide nanoparticles. Radiation-induced formation of monodisperse CdS, ZnS, PbS nanoparticles is usually performed in presence of thiol compounds [124–128], and on the whole the process goes on by one-type mechanism [129]. Irradiation of solution containing a polar solvent causes formation of active

particles. Among them a hydrated electron having most strong reducing properties interacts with thiols by the following scheme:

$$HOCH_2CH_2SH + e_{aq}^- \rightarrow {}^{\bullet}CH_2CH_2OH + HS- \quad (3.31)$$

$$HOCH_2CH_2SH + OH^{\bullet} \rightarrow {}^{\bullet}SCH_2CH_2OH + H_2O \quad (3.32)$$

$$Pb^{2+} + OH^{\bullet} \rightarrow Pb^{3+} + OH^- \quad (3.33)$$

with the rate constants $k_1 = 1.2 \times 10^{10}$ M^{-1} s^{-1}, 6.8×10^9 M^{-1} s^{-1} и $< 2 \times 10^8$ M^{-1} s^{-1}, respectively.

Monomer sulfide forms when Pb^{2+} reacts with HS^-:

$$Pb^{2+} + HS^- \rightarrow PbS + H^+ \quad (3.34)$$

with the following coalescence and formation of a nanoparticle with radiation yield 2.7×10^{-7} mol·J^{-1} [129]:

$$n\text{PbS} \rightarrow (\text{PbS})_n \quad (3.35)$$

When $Na_2S_2O_3$ is used as a sulfiding agent at producing of chitosan-ZnS and chitosan-ZnS:Mn^{2+} [130] the reduction reaction of ${S_2O_3}^{2-}$ can proceed with participation of e_{aq}^- or atomic hydrogen:

$${S_2O_3}^{2-} + 2e_{aq}^- \rightarrow {SO_2}^{-3} + S^{2-}, \quad (3.36)$$

$${S_2O_3}^{2-} + 2H^{\bullet} \rightarrow {SO_3}^{2-} + 2H^+ + S^{2-}, \quad (3.37)$$

$$S^{2-} + Zn^{2+} + Mn^{2+} \rightarrow ZnS : Mn^{2+}, \quad (3.38)$$

$$n(ZnS : Mn^{2+}) \rightarrow (ZnS : Mn^{2+})_n. \quad (3.39)$$

The absorbed dose and irradiation power are important factors of control over sizes of formed nanoparticles and, finally, over their optical properties. ZnS nanoparticles were synthesized by γ-irradiation of water solution containing Zn^{2+} and thiol (RSH) [129]. Under low irradiation doses monodisperse ultra fine ZnS particles with diameter 1.5 nm form and absorption band appears at the wavelength 238 nm. Coarser nanoparticles form under higher doses with absorption at $\lambda > 260$ nm.

By change in irradiation dose, not only sizes of nanoparticles change, but, respectively, photoluminescent properties of the nanocomposites. Thus, the photoluminescent peak in ZnS-chitosan emission spectrum is barely seen under irradiation by 5 kGy dose, but at the dose 10 kGy quantum yield is 16.6 %, and emission peak appears at 442 and 584 nm. As irradiation dose increases, sizes of nanoparticles increase and photoluminescent emission peak reaches 22.5 %, and as the dose increases further on to 30 Gy, the yield begins to decrease, which is caused by breakage of a crystal structure of chitosan.

It should be noted that obtained by radiolysis nanocomposites of the considered type (quantum dots in biocompatible polymer matrix) are, as a rule, well dissolved in water. In combination with efficient luminescent properties these materials are interesting for different biomedical applications [131, 132]. The CdS polyamidoamine dendrimer with terminal amino- and carboxyl groups obtained from $CdCl_2$ solution and a polymer in presence of sodium thiosulfate under action of ^{60}Co-γ-source is tested for detection of ascorbic acid in pharmaceutical drugs [128]. Ability to detect ascorbic acid in micromolar concentrations is caused by efficient extinguishing of luminescence of a nanocomposite biosensor by the acid. However, even more than 100-fold concentration excess of ordinary interfering agents such as tartaric, uric, citric, acetic acids had no significant effect on fluorescence of the nanocomposite.

3.3.4 Synthesis of Bimetallic Nanocomposites

The method of radiolytic reduction is especially attractive for production of heterometallic nanocomposites. Nanoparticles consisting of two or more different metals are of a special interest for development of materials with new properties, because at the nanoscale intermetallic compounds and alloys can be obtained, which do not form in the case of compact metals. Radiation reduction of salt solutions was used to obtain nanoparticles including two [133–135] and three [136] metals. General strategy for producing these nanocomposites is analogous to the above mentioned and includes incorporation of metal ions in a solution or suspension of a matrix polymer and the following reduction by γ-irradiation. Chemical bonding of metal ions with matrix promotes yield and homogeneous distribution of nanoparticles in volume on a substrate surface, as it is shown in the system multiplayer carbon nanotubes-sulfided polyaniline alloy – Fe-Pd nanoparticles (Scheme 3.11) [134]:

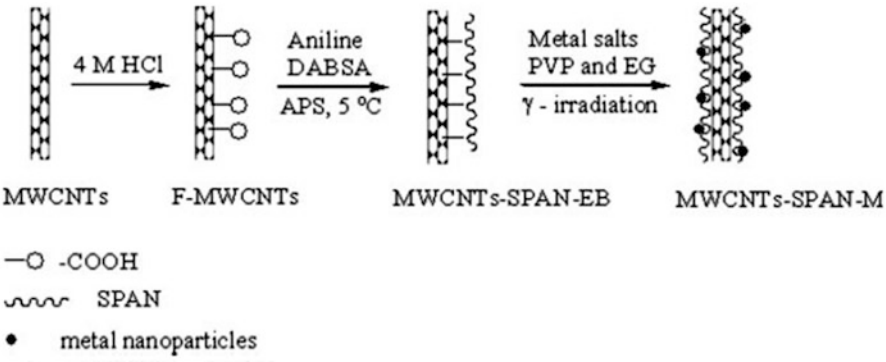

2,5-Diaminobenzene sulfonic acid (DABSA), carboxylic acid functionalized MWCNTs is F-MWCNTs, ammonium peroxydisulfate $[(NH_4)_2S_2O_8)]$ or APS.

Scheme 3.11 Preparation of multilayered carbon nanotube-sulfonated polyaniline-Fe-Pd alloy nanocomposites

It should be noted that conductivity of this composite was 1.5 S cm^{-1}, which was far higher than conductivity of SPAN ($2.46 \cdot 10^{-4}$ S cm^{-1}).

Advantage of radiolytic method of production of heterometallic nanocomposites is that using of powerful irradiation dose makes it possible to reduce a metal ion very rapidly, and thus to prevent electron transport between metals. Therefore, it is possible to obtain desirable structures of core-shell or homogenous alloy nanoparticles. This strategy is successful in production of nanocomposite alloys, which are difficult to obtain from non-mixed metals in bulk state, as in case, for example, of Ag and Ni. Radiolytic synthesis of Ag-Ni alloy of different stoichiometric compositions and of $Pd_{0.5}$-$Ni_{0.5}$ alloy was performed successfully at room temperature [137]. Oppositely to thermodynamically stable core-shell structure of Ag-Ni nanoparticles, kinetically preferable phase with average particle diameter 5.8 nm and narrow distribution forms in $Ag_{0.5}$-$Ni_{0.5}$ under high irradiation dose (power 300 rad/s) [138]. Properties of the formed bimetallic nanoparticles and nanoalloys are predominantly conditioned by their structures, which are far more complex than those of monometallic particles. These structures include core-shell and subcluster-segregated alloys ordered or heterogeneously mixed nanoalloys, etc. Their particular feature is wide variety of shapes. Apart from spherical nanoparticles, under radiolysis conditions bimetallic nanostructures with high aspect ratio can form. Whiskers nanocrystalline structures of several microns in length and from 3 to 20 nm in diameter were produced by radiation reduction of Ag^+ и $PtCl_6^{2-}$ ions in water solution and in presence of the stabilizer, polyvinyl alcohol with a different degree of hydrolysis [139]. The crucial role in formation of nanowires has molar ratio of two metals and formation of metal-polymer complexes. It is assumed that presence of hydrophilic alcohol and hydrophobic acetate PVA groups can have an effect on anisotropy of formed structures during radiolysis reduction.

3.3.5 *In Situ Radiolysis*

Original possibility of using *in situ* radiation source (oppositely to exterior source), on the one hand, and production of radioactive nanoparticles, on the other hand, was demonstrated on the example of $H^{198}AuCl_4$ served as a precursor for synthesis of Au nanoparticles in polyethylene glycol [140]. Products of PEG and H_2O radiolysis formed under impact of γ-energy of ^{198}Au (411 keV) stimulate reduction of a metal ion with the following stabilization of PEG by the similar mechanism considered above for the cases of external irradiation. It should be noted that the obtained radioactive nanoparticles have high energy of γ-radiation ($\tau_{1/2} = 2.69$ day) and can be used *in vivo* and *in vitro* for different biomedical purposes (see Chap. 7), even more that the described method allows production of nanoparticles with rather high concentrations. It is interesting that *in situ* radioactivity of ^{198}Au isotope was also efficient in synthesis of Au-Pd bimetal nanoparticles with core-shell structure [141], despite essentially low radiation doses (0.01 mCi), as compared, for example, with very high irradiation power density up to $9 \cdot 10^2$ Gy/h for ^{60}Co γ-beams also used for production of bimetal nanoparticles [135].

3.4 Sonochemical Reduction

Sonochemistry is based on the acoustic cavitation phenomenon, which includes nucleation, growth and collapse of bubbles in liquid medium. Almost adiabatic collapse of microbubbles in a solution brings to rise in local temperatures up to (>5,000 K), pressure (>20 MPa), and cooling rate ($>10^7$ K s^{-1}) in micro-environment from 0.3 to 150 μm depending on ultrasonic frequency (5 MHz, 20 kHz) [142]. On the gas/liquid interface free radicals form, which induce sonochemical reactions. Different types of particles and reducing agents form during sonolysis of water and organic compounds (2-propanol,[3] ethylene glycol, surfactants, polymer molecules, etc.). Extreme conditions formed under impact of ultrasonic wave are widely used to produce different metal-containing nanoparticles and nanocomposites [143–146]. Sonochemical reduction of metals includes three main stages: formation of active particles, reduction of metal, and growth of these particles. These processes can take place in different media: in gas medium of cavitation bubbles under impact of high temperature and pressure water undergoes pyrolysis, as a result, H and OH radicals form on the interface between the bubbles and the solution, and finally in the solution (Scheme 3.12) [147].

Scheme 3.12 The main stages of sonochemical reduction

Generation of active species:

In cavitation bubbles:

$$H_2O \xrightarrow{\text{Ultrasound}} H^{\bullet} + OH^{\bullet}$$

At bubbles/solution interface:

$$RH \xrightarrow{\text{Ultrasound}} R_1^{\bullet} + H^{\bullet}$$

$$OH^{\bullet}(H^{\bullet}) + RH \longrightarrow R_2^{\bullet} + H_2O\ (H_2)$$

Metal reduction:

In solution:

$$M^{n+} + nR_1^{\bullet}(R_2^{\bullet}) \longrightarrow M^0 + nR_1^{\bullet}(R_2^{\bullet}) + nH^+$$

Growth of colloids:

In solution:

$$nM^0 \longrightarrow M^0{}_{\text{colloid}}$$

Due to low vapor tension of metal salts, reduction proceeds mainly on the bubbles/solution interface. The important factors, which influence efficiency of cavitation and physical-chemical properties of the products, are power and frequency of ultrasonic action, temperature of the initial solution, character of a solvent, etc. It has been

[3] This is most often used organic addition is involved in sonochemical reactions as a polar solvent having lower boiling temperature and surface tension than water, but with higher vapor tension to change parameters of gas/liquid interface and to increase energy yield.

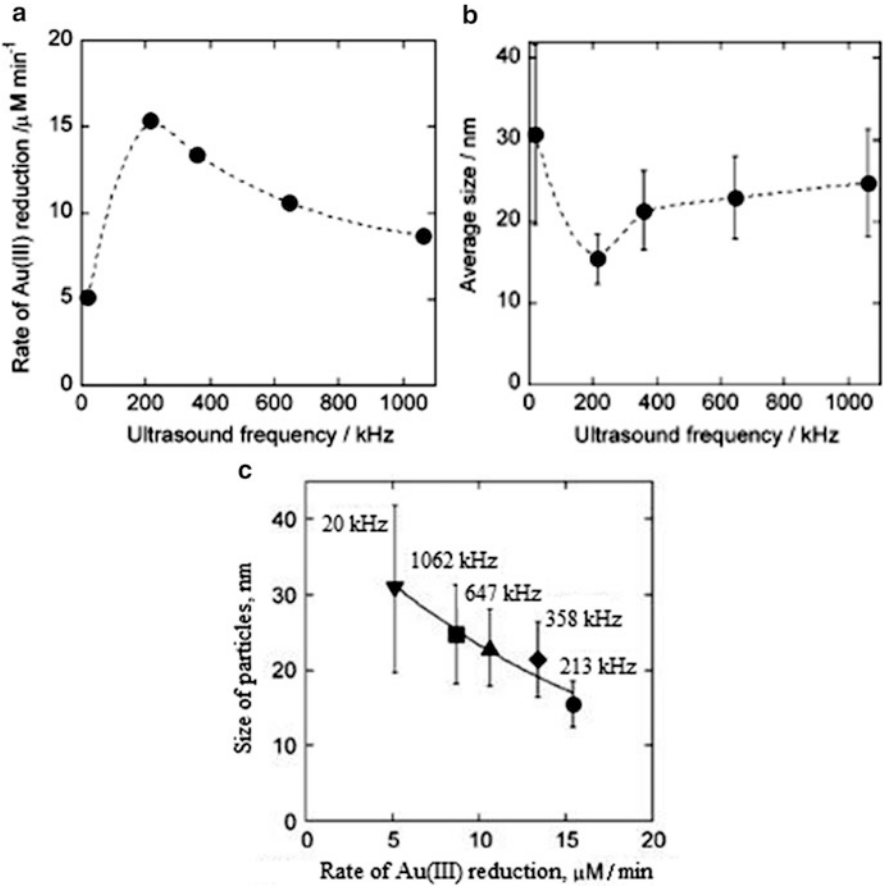

Fig. 3.7 Dependence of the reduction rate of Au(III) on ultrasonic frequency (**a**) and average size of the particles as a function of ultrasonic frequency (**b**) and of the reduction rate of Au(III) (**c**). Conditions: Au(III): 0.2 mM, 1-propanol: 20 mM, Ar, power of ultrasound is 0.1 W ml^{-1} [148]

shown that during sonochemical reduction of Au(III) in water solution containing 1-propanol, the initial rate of the reaction depends significantly on frequency of ultrasound [148]. As is seen from Fig. 3.7, the reduction rate decreases as ultrasonic frequency increases. It should be noted that size of the formed Au particles is predominantly determined by the reaction rate and almost does not depend on frequency of ultrasonic field. This confirms that sonochemical nucleation and growth processes of metal clusters and nanoparticles are slightly influenced by mechanical forces formed during cavitation [145].

However, in the case of Zn, Cr, Ni, and Mo metal particles with the sizes from 5 to 10 μm there were agglomeration/melting processes and necks formed between the particles due to local melting induced by high velocities of collisions between particles under impact of intense shock wave at 20 kHz ultrasonic frequency [149]. Moreover, 20-min impact of highly intense (40 W cm^{-2}) ultrasonic wave of

the same frequency on the previously obtained citrate-preserved Au nanoparticles with the average diameter 25 ± 7 nm was enough to cause melting of nanoparticles in the zone of contacts and formation of dumb-bell like structures [150].

Comparison of the boundary layer thickness δ, tangential velocity near the bubble surface υ_t and the resulting shear stress Ψ found from the expressions (3.40, 3.41 and 3.42):

$$\delta = \sqrt{\frac{2\eta}{\rho\omega}} \tag{3.40}$$

$$\upsilon_t \approx \frac{\omega\xi^2 R_0^4}{r^5} \Rightarrow \frac{\omega\xi^2}{R_0} \tag{3.41}$$

$$\psi = \eta\frac{\partial \upsilon_t}{\partial r} \approx \frac{\eta\omega\xi^2}{R_0\delta} \tag{3.42}$$

where η and ρ are viscosity and density of water at room temperature, respectively, R_0 is equilibrium radius of the bubble, ξ is displacement amplitude and ω is frequency of ultrasonic wave has shown that tangential velocity υ_t and shear stress Ψ for the system under action of 200 kHz ultrasonic wave are by 3–4 orders of magnitude lower than in the case of the ultrasonic wave at 20 kHz frequency. This confirms that physical effects caused by ultrasound should be far more prominent in the latter case than at frequency 200 kHz and above. We shall also note that these conclusions agree well with the abovementioned examples of Au nanoparticles with the average size from 15 to 25 nm non-melted under ultrasonic impact in the frequency range from 213 to 1,062 kHz [148].

The method of sonochemical synthesis is also successfully used to obtain bimetallic systems. Morphological core-shell structures can be produced by consequent reduction as, for example, in the case of Pt-Rh nanostructure [151], or by simultaneous treatment in ultrasonic field of solution of mixture of metal ions as was shown for Au and Ag [152, 153]. The decisive role in core-shell formation of the structure plays reduction rate of a metal ion under conditions of sonochemical reaction and the character of stabilizing of a polymer matrix and formation of polymer-metal ion complex.

The approaches are intensely studied, which combine advantages of sonochemical reactions with other methods. Among them sono-electrochemical methods can be distinguished, their advantages are acceleration of mass transport, cleaning and degassing of the surface of electrodes, increase in reaction rates, etc. Pulse sono-electrochemical method has been successfully used for production of nanostructural materials, it is based on alternating impact of sonic and electric pulses on a reacting system [154, 155]. Initially metal or semiconductor particles were electro-deposited, then shock ultrasonic wave was applied to remove the particles from the electrode surface. This way fine Pd particles of different morphologies and sizes were obtained [156], as well as Ag [157] and Cu [158] in

Table 3.8 Effect of various deposition parameters on Cu particle size [158].

Variable parameter	Conditions	Particle size, nm
Current density, mA/cm^2	55	29 ± 2
	70	24 ± 4
	100	10 ± 2
Reaction duration, min	10	23 ± 2
	30	29 ± 2
	60	38 ± 4
PVPr concentration, %	0.2	55 ± 10
	1	33 ± 2
	2	29 ± 2
Temperature, °C	15	17 ± 3
	25	29 ± 2
	50	62 ± 5
Ultrasound power, W	35	29 ± 2
	50	29 ± 2
	76	29 ± 2

presence of poly (N-vinylpyrrolidone) (PVP). Sizes of the nanoparticles and their morphologies are controlled by change in reaction conditions (Table 3.8).

It draws attention that in many sonochemical reactions often poly (N-vinylpyrrolidone) is used as a stabilizing agent. Moreover, it is assumed that presence of shear stresses of a polymer in water solution can also induce sonochemical reaction in flowing medium [159]. The stabilizing mechanism of PVP action is based on specific structure of its molecule including polar functional groups, which can donate unpaired electron forming coordination bond with a metal ion, and which after reduction can also form bonds with clusters and metal nanoparticles preventing further aggregation of both as is shown in the sonochemical synthesis of Cu nanoparticles (Scheme 3.13) [158]:

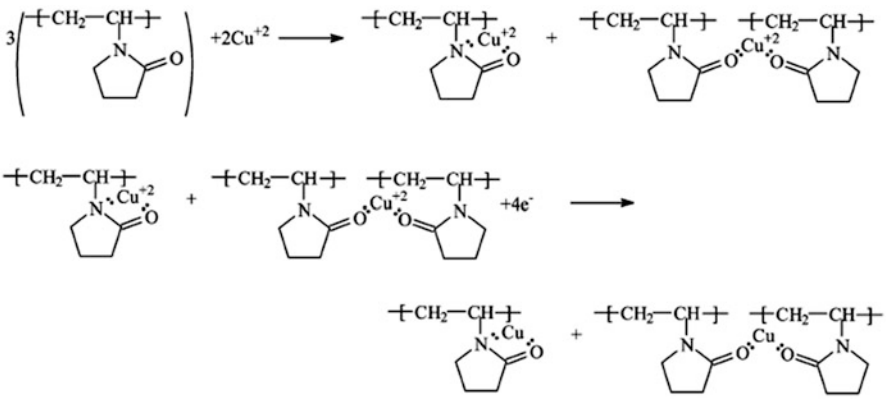

Scheme 3.13 Forming of complexes of Cu^{2+} ions and Cu nanoparticles with poly (vinylpyrrolidone)

Table 3.9 Characteristics of the Pd/PVP nanocomposite obtained by a sonochemical reaction [163].

Concentration of Pd(II) $\times 10^3$, mol.	Average size of particles, nm	Calculated number of particles	Global particle surface, nm^2	$PVP_n/N_{particles}$	$PVP_n/S_{particles}$, molecules/nm^2
0.66	3.5	$0.26 \cdot 10^{18}$	$9.87 \cdot 10^{18}$	11.74	0.31
1.33	4.5	$0.24 \cdot 10^{18}$	$15.46 \cdot 10^{18}$	12.38	0.19
2.0	5.5	$0.19 \cdot 10^{18}$	$17.74 \cdot 10^{18}$	16.12	0.17
2.66	2.5	$2.84 \cdot 10^{18}$	$55.67 \cdot 10^{18}$	1.06	0.05

A large body of FT-IR spectral research [160–162] has shown that in the range of valence vibrational modes of the carbonyl group of poly (4-vinylpyrrolidone) 1,665–1,640 cm^{-1} there is displacement to low frequency region, which points to the interaction between C = O and surface of nanoparticles. The absorption band of the carbonyl group in the Pd(II)- poly (4-vinylpyrrolidone) system depends on concentration of a metal ion, i.e. on a number of particles in suspension [163]. A change in the initial concentration of Pd(II) from $0.66 \cdot 10^{-3}$ to $2 \cdot 10^{-3}$ mol brings to increase in size of Pd nanoparticles from 3–4 nm to 5–6 nm. The respective increase in the molar ratio Pd(II)/PVP is reflected in a decrease in number of nanoparticles, and for the maximum ratio Pd(II)/PVP there is maximum number of particles, therefore PVP cannot cover every particle (Table 3.9).

The active medium for sonochemical reactions are ionic liquids such as 1-n-alkyl-3-methylimidazolium- bis(trifluoromethanesulfonyl)imide, etc. [164, 165]. Non-traditional class of solvents containing organic cations such as imidazolium, pyridinium, pyrrolidinium, quaternary ammonium, sulfonium, and inorganic anion attract attention by their chemical stability at high temperatures, low volatility, low toxicity and low flammability, i.e. they mostly meet demands of green chemistry. By varying length of alkyl chain and duration of ultrasonic action it is possible to control efficiently morphology and sizes of nanoparticles, for example, to obtain ZnO in form of nanorods or nanosheets [166]. It should be noted that sonochemical synthesis, as a rule, brings to products with lower crystallinity than traditional heating methods. Therefore sometimes sonochemical reactions are performed at high temperatures. Thus, increase in temperature from room temperature to 40–100 °C for production of Mn_3O_4 colloid nanoparticles leads to considerable improvement of crystallinity of the product, though in the absence of ultrasonic impact completely amorphous colloid nanoparticles are formed (Fig. 3.8) [167].

Therefore, sonochemical approach has wide application due to low cost and high efficiency of the procedure of ultrasonic cavitation. On the other hand, impact waves and turbulent flows generated by multiple collapses of microbubbles, make nanoparticles move with velocities of hundreds meters per second and undergo non-elastic impact with change in shape and crystallinity, i.e. ultrasonic melting of inorganic materials provides production of metal particles at the nanoscale with different morphologies and properties.

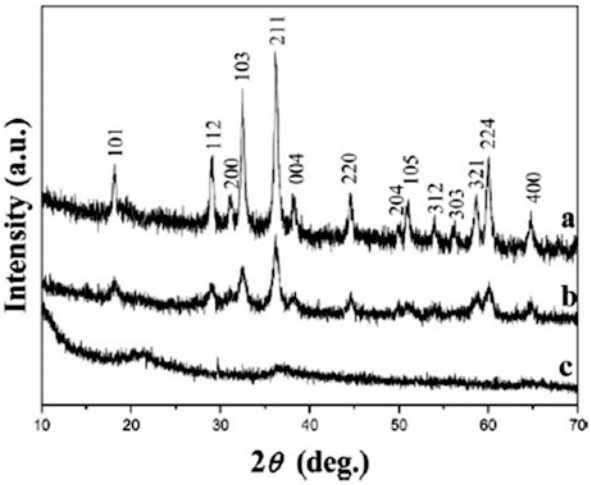

Fig. 3.8 X-ray diffraction patterns of the samples of Mn_3O_4 colloid nanoparticles synthesized at: (*a*) 100 °C, (*b*) room temperature, (*c*) at room temperature without ultrasonic impact [167]

Sonochemical methods include unique reaction ways for development of different kinds of composite materials [148, 168–171]. Sonochemical intercalation of Au nanoparticles in interlayer space of Na-montmorillonite can be a general approach to synthesis of thermally stable metal-clay nanocomposites with high dispersion ability of metal nanoparticles, including catalytically active [172]. Important advantage of ultrasonic treatment is its multifunctional character, which displays itself in a possibility to perform different procedures under its action: dispersion, emulsification, organic synthesis, and polymerization. Combination of dispersion and polymerization processes *in situ* were used to obtain polyaniline/Fe_3O_4 [173] and poly (n-butyl methacrylate)/γ-Al_2O_3 nanocomposites [174]. In the latter case encapsulated polymerization induced by ultrasonic irradiation (at frequency $2 \cdot 10^4$–10^9 Hz) proceeds with high conversion in presence of sodium dodecyl sulfate in the system, which points to the fact that radicals which induce emulsion polymerization of butyl methacrylate form during dissociation of a surfactant.

On the whole, sonochemical method of nanocomposite production can be considered as one of the most attractive and in this view it serves as an alternative to ordinary solvothermal or hydrothermal synthesis, sol-gel processes, co-deposition, electrochemical and pyrolytic methods. Most of these synthetic methods need high temperatures, involve metal-organic precursors sensitive to oxidizing media and temperature, and often use environment-polluting agents, etc. [175].

3.5 Physical and Chemical Deposition from the Vapor Phase

Different variants of techniques of deposition from vapor phase are widely used for production of metal polymer nanocomposites [4, 176, 177]. Their essence is in simultaneous or consequent deposition of metal and organic components and

formation of metal nanoparticles in growing composite films. Active metal atoms during collision with polymer surface can diffuse in volume of a polymer matrix, be captured by surface defects, and collide with each other, which results in aggregation and formation of cluster particles. The volume fraction of metal nanoparticles in a polymer film can be controlled by relationship between deposition rates of metal and polymer components [178]. We shall consider some ways of production of nanocomposites.

3.5.1 Plasmochemical Synthesis

In this method low temperature (4,000–10,000 K) nitrogen, ammonium, hydrogen, hydrocarbon, or argon plasma is used, which is generated by arc, glow, high-frequency or microwave discharge. The main conditions for obtaining nanoparticles by this method are the reaction process being far from equilibrium, high rate of the solid-state phase nucleation and low growth rate. Plasma chemical synthesis provides high rates of formation and condensation of a compound and quite high efficiency. Due to these advantages plasma technology is widely applied in production of nanostructural materials [179, 180].

The method of plasma condensation is one of universal methods for production of metal polymer nanocomposites based on spraying of a metal target and simultaneous polymerization of organic precursors in plasma [5, 176, 181]. This approach supplies production of homogeneously distributed nanoparticles in a polymer matrix and provides variation of degree of filling in wide range. Most often fluorocarbon [182], hydrocarbon [182–185], organosilicic [186, 187] precursors are used for production of polymer matrix. The Ti- [184] and Pt- [185] hydrocarbon nanocomposite coatings were obtained by one-stage plasma polymerization method.

Content, size and distribution of metal clusters depend on parameters of plasma chemical process, and can be regulated by power of plasma supply and flow velocity of a monomer (Fig. 3.9).

Among plasma-mediated methods there are interesting approaches based on use of monodisperse metal clusters generated in separate reactors by mechanism of gas aggregation in connection with filtration by mass [188–191]. Formation of clusters carries on in an aggregation chamber during thermal evaporation of a metal into flow of a carrier gas (Ar or He) under high pressure (~100 Pa). Metal atoms are condensed on gas molecules, and the generated clusters grow during homogeneous nucleation-condensation and evaporation of atoms. The formed clusters are transferred with the gas-carrier flow through the outlet nozzle to substrate in the reactor, where a polymer condenses gradually during plasma polymerization (Fig. 3.10).

It is interesting that the obtained by this strategy Pd cluster structures on PMMA display far higher adhesion than the metal films synthesized by thermal evaporation [192]. This method provides development of 3D nanocomposites with homogeneous size distribution of nanoparticles in volume of a polymer matrix, and

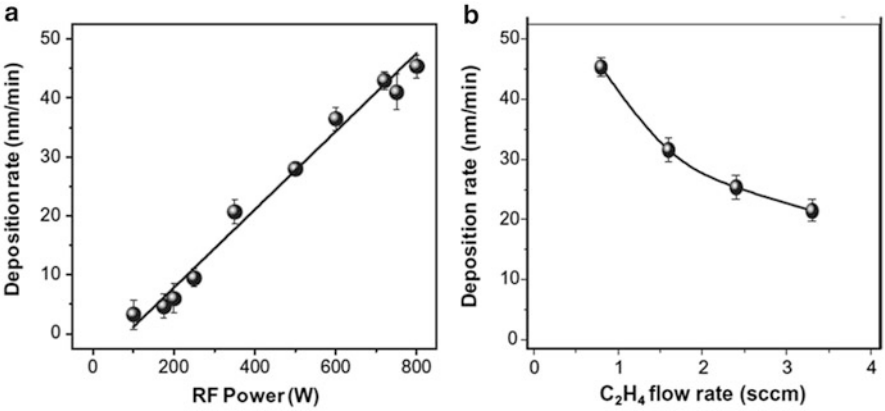

Fig. 3.9 Deposition rate of Pt/CH_x nanocomposite film vs. input power (**a**) and ethylene flow rate (**b**) [185]

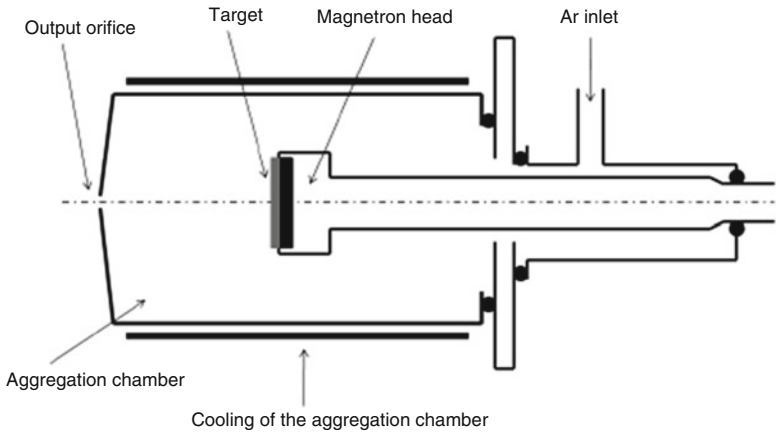

Fig. 3.10 Schematic drawing of reactor for synthesis of monodispersed metallic cluster by thermal evaporation and gas aggregation [188]

development of layered nanocomposite structures. In the latter case necessary concentrations are achieved by variations of deposition time, while for bulk deposition it is important that the deposition rate of a polymer was higher than the deposition rate of the clusters, like in $Ag/SiO_xC_yH_z$ [191].

3.5.2 Evaporation and Spraying Methods

The condensation (deposition) method from the vapor phase used for production of metal polymer nanocomposites is usually reduced to evaporation of a monomer and

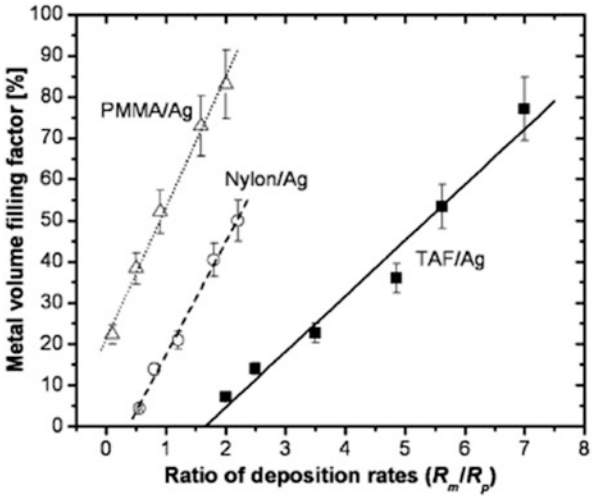

Fig. 3.11 The volume fraction of Ag in nanocomposites versus ratio of evaporation rates Rm/Rp of Ag to TAF (1), Nylon (2), and PMMA (3), respectively [178]

poly-condensation on a substrate, thermal disintegration of some polymers, for example, Teflon, and partial repolymerization of fragments on a substrate [4, 177, 193]. Nanocomposite materials with different content of metal are obtained by simultaneous deposition of noble metals and polymers (nylon 6, polytetrafluoroethylene, PMMA) [178]. Increase in particle size with increase in metal concentration is typical of vapor deposition, in which temperature can be used as additional controlled parameter. Volume fraction of a metal in nanocomposite depends almost linearly on the ratio of metal/polymer deposition rates (Fig. 3.11).

The considered technique can also be used to obtain nanocomposite films containing bimetal nanoparticles. The co-evaporation and co-deposition methods were used to synthesize Au_xAg_{1-x} [194] and Cu_xAg_{1-x} [195] in Teflon polymer matrix. Components of the formed nanocomposite were evaporated simultaneously from separate targets in a chamber under residual pressure 2.4×10^{-5} Pa. Despite of a complicated character of the processes in these systems (absorption and reemission of metals, surface diffusion, etc.), coefficients of condensation can reach 60 %, nanocomposite films are characterized by homogeneous size distribution of particles in the matrix (Fig. 3.12) in a wide range of their compositions and volume fractions. The nanodisperse phase has prevailingly a core-shell structure, which forms, probably, due to a considerable difference between coefficients of condensation, for example, between copper and silver atoms.

Methods of simultaneous and consequent spraying and condensation include radio frequency (RF) magnetron spattering of polymers from a polymer target and cathode spattering of a metal target with direct current (DC) energy supply. Under RF impact a polymer is fragmented and linked, which can bring to improvement of mechanical properties of the obtained nanocomposite materials. The most often used polymers in this technique are polytetrafluoroethylene and nylon [196, 197]. It should be noted that this approach is especially efficient for production of alloys of

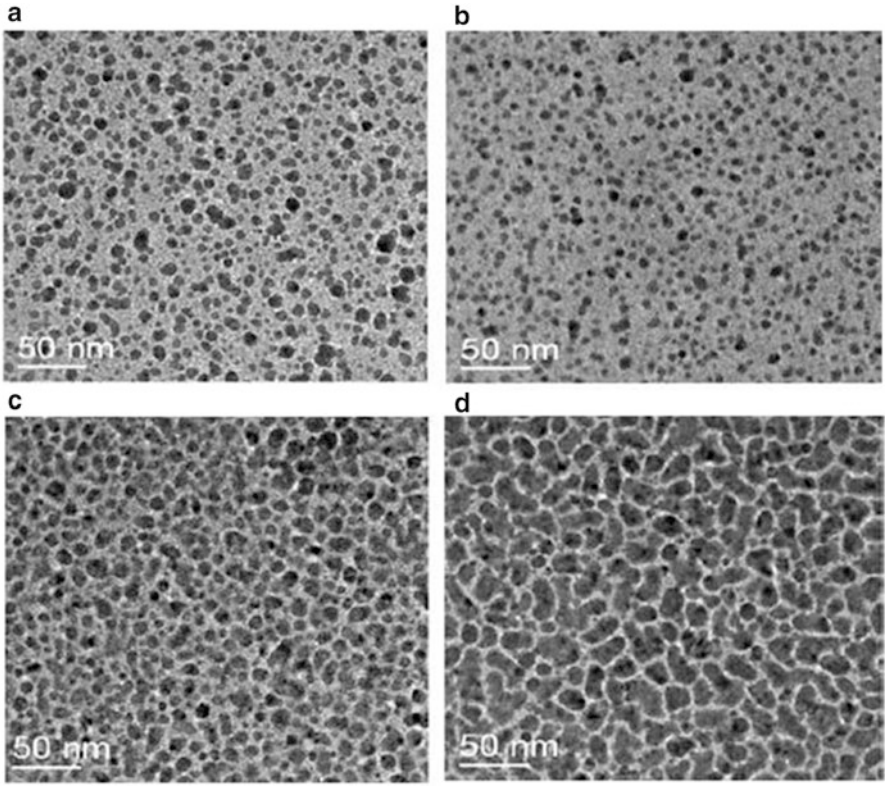

Fig. 3.12 TEM micrographs of bimetallic Cu_xAg_{1-x}/teflon nanocomposites with different composition (x) and volume fraction (f) of nanodispersed phase: (**a**) x = 0.2, f = 17 %; (**b**) x = 0.31, f = 17 %; (**c**) x = 0.34, f = 42 %; (**d**) x = 0.35, f = 54 % [195]

bimetallic nanoparticles on the surface of polymers, as has been shown in the case of Au-Ag/PTFE nanocomposites [194, 198], while consequent deposition processes, as a rule, bring to formation of core-shell structures, and in this case additional treatment is needed for production of alloyed particles, for example, annealing [199] or laser-induced melting [200]. A possibility of use of targets made of pure metals [201] and their alloys [202] is shown. The TiO_2/FeCo nanocomposite was produced one stage by simultaneous DC spraying of FeCo target and TiO_2-RF magnetron spattering [203].

An interesting approach was realized in multilayered nanocomposite material based on Ag-composite [204]. Hydrophilic polymer layer, composition and thickness of which was controlled by O_2 flow during polymerization, was formed by plasma polymerization of hexamethyldisiloxane (HMDSO) on the surface of Ag nanoparticles of 2D ensemble in a thin layer of RF-spattered PTFE (Fig. 3.13).

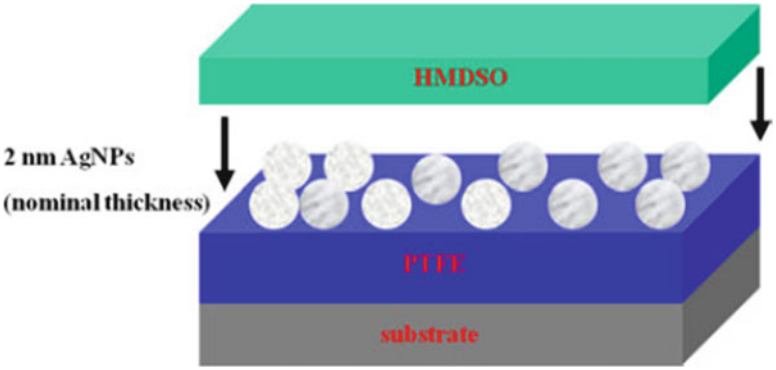

Fig. 3.13 A schematic view of the multilayered HMDSO/Ag/PTFE nanocomposites [204]

Microstructure and thickness of plasma-polymerized polymer film have a significant effect on properties of multilayer composite material, in particular, on release of silver ions.

3.5.3 Laser Ablation

Laser ablation of solids in liquid attracts more and more interest in production of nanoparticles [4, 205–207]. The essence of this method is in focusing laser beam through a transparent liquid to a metal target surface. Interaction of a powerful laser irradiation with absorbing media causes ablation of the latter and spattering of their material in air. At high absorption coefficients thickness of the removed layer is small, from units to tens nanometers. Nanoparticles form due to collision of molecules of a substance with each other during adiabatic expansion and recombination of plasma flame in rarefied gas. Mean free path of molecules is in the case of laser ablation of solids in liquids by several orders of magnitude lower than that in vacuum, because evaporated material of the target collides with vapors in the liquid near the target. High pressure of liquid vapors at the temperature of the target has effect on size distribution of the particles. Moreover, the function of size distribution of the particles can vary during irradiation due to absorption at the wavelength of laser irradiation. One of advantages of this method is the fact that synthesis of metal colloids can be realized in a solution in absence of chemical reagents, i.e. high purity grade products can be obtained.

Laser ablation in presence of surfactants and polymers brings to formation of nanocomposite materials. Microstructure of the obtained nanocomposites is substantially affected by parameters of laser interaction. Granular magnetoresistive Co/PTFE nanocomposites are obtained by laser ablation (Nd-YAG laser at the temperature 355 nm) [208]. Colloids of silver nanoparticles obtained by laser irradiation in water solution of polyvinylpyrrolidone were more stable than

colloidal water solutions [209]. Method of pulse laser ablation make it possible to carry out functioning of nanoparticles by direct incorporation of functional agents in ablation medium before laser irradiation, thus favoring simultaneous generation of a nanoparticle and covalent bonding of a ligand, especially this approach is important for production of bionanocomposite materials (see Chap. 7) [210, 211]. In situ bonding of laser generated Au nanoparticles by functional biomolecules is shown for dextran-coated nanoparticles used as biosensors for lectins [212]. Another similar example relates to conjugation of Au nanoparticles with thermo-sensitive co- poly(N-isopropylacrylamide) polymer with terminal thiol groups in the processes of in- and ex-situ laser ablation [213]. Undoubtedly, in systems containing thermo-sensitive biomolecules it is necessary to take into account degrading effect of laser on them [214].

Theoretical studies in the field of applications of low temperature plasma in nanotechnologies are intensely carried on. The theoretical model is developed to estimate typical sizes of nanostructures formed on the surface of solids during melting under laser irradiation [215]. Solution of Stefan problem of melting and crystallization of the surface layer in combination with the theory of formation of crystal nuclei displays a dependence of cooling rate and typical sizes of the seeds on pulse duration and energy. At duration 10^{-8} s and energy density 4 J/cm^2 the calculation gives typical sizes of the structures about interatomic distances (5×10^{-10} m), while at duration 10^{-6} s and energy 6 J/cm^2 the typical size is ~100 nm.

Resuming, it can be noticed that classical solution methods for production of nanocomposite materials, such as sol gel synthesis (see Chap. 4), hydrothermal methods, etc., become more and more differentiated, and preparative instrumentation is supplemented by innovation approaches, such as microwave, laser, sonic-chemical techniques, etc. For example, metal nanoparticles incorporated in dielectric nanofibers are obtained in a sandwich-like microreactor by combined application of H_2 plasma of high-frequency microwave power and high temperature of substrate [216]. In order to develop inorganic n-p-hetero-junctions based on GaN/InGaN 1D heterostructures, the method of plasma-mediated molecular-beam epitaxy was successfully used [217]. In similar semiconductor structures TiO_2 shell was formed by plasma spattering on the surface of ZnO nanorods, preliminary obtained by hydrothermal method [218].

A tendency of development will, probably progress towards combination of new synthetic strategies and hybrid approaches with individually adapted instrumentation for design of technologically important nanostructural materials.

References

1. C. Boissiere, D. Grosso, A. Chaumonnot, L. Nicole, C. Sanchez, Adv. Mater. **23**, 599 (2011)
2. G.R. Patzke, Y. Zhou, R. Kontic, F. Conrad, Angew. Chem. Int. Ed. **50**, 826 (2011)
3. I. Marozau, A. Shkabko, G. Dinescu, M. Dobeli, T. Lippert, D. Logvinovich, M. Mallepell, C.W. Schneider, A. Weidenkaff, A. Wokaun, Appl. Surf. Sci. **255**, 5252 (2009)

4. F. Faupel, V. Zaporojtchenko, T. Strunskus, M. Elbahri, Adv. Eng. Mater. **12**, 1177 (2010)
5. A. Heilmann, *Polymer Films with Embedded Metal Nanoparticles* (Springer, Berlin, 2003)
6. M. Baghbanzadeh, L. Carbone, P.D. Cozzoli, C.O. Kappe, Angew. Chem. Int. Ed. **50**, 11312 (2011)
7. M. Tsuji, M. Hashimoto, Y. Nishizawa, M. Kubokawa, T. Tsuji, Chem. Eur. J. **11**, 440 (2005)
8. A.S. Vanetsov, Yu.D. Tret'yakov, Uspekhi Khim. **76**, 435 (2007)
9. Y. Bykov, K.I. Rybakov, V.E. Semenov, Russ. Nanotechnol. **6**, 60 (2011)
10. Y.I. Bokhan, I.A. Shkreb, Pis'ma v ZHETF **20**, 24 (1994)
11. Y.V. Bykov, K.I. Rybakov, V.E. Semenov, J. Phys. D **34**, R55 (2001)
12. H.M. Kingston, S.J. Haswell (eds.), *Microwave-Enhanced Chemistry* (American Chemical Society, Washington, DC, 1997)
13. J. Park, J. Joo, S.G. Kwon, Y. Jang, T. Hyeon, Angew. Chem. **119**, 471 (2007)
14. I. Pastoriza-Santos, L.M. Liz-Marzan, Langmuir **18**, 2888 (2002)
15. M.N. Nadagouda, R.S. Varma, Cryst. Growth Des. **8**, 291 (2008)
16. B. Baruwati, V. Polshettiwar, R.S. Varma, Green Chem. **11**, 926 (2009)
17. M.N. Nadagouda, R.S. Varma, Biomacromolecules **8**, 2762 (2007)
18. M. Tsuji, M. Hashimoto, Y. Nishizawa, T. Tsuji, Chem. Lett. **32**, 1114 (2003)
19. B. Baruwati, M.N. Nadagouda, R.S. Varma, J. Phys. Chem. C **112**, 18399 (2008)
20. X. Zhu, J. Wang, Z. Zhang, J. Zhu, S. Zhou, Z. Liu, N. Ming, J. Am. Ceram. Soc. **91**, 2683 (2008)
21. L.T. Guo, H.J. Luo, J.Q. Gao, L.Z. Guo, J.F. Yang, Mater. Lett. **60**, 3011 (2006)
22. B.L. Newalkar, S. Komarneni, H. Katsuki, Mater. Res. Bull. **36**, 2347 (2001)
23. W. Sutton, Ceram. Bull. **68**, 376 (1989)
24. D. Li, S. Komarneni, J. Am. Ceram. Soc. **89**, 1510 (2006)
25. H. Grisaru, O. Palchik, A. Gedanken, V. Palchik, M.A. Slifkin, A.M. Weiss, Y. Rozenfeld Hacohen, Inorg. Chem. **40**, 4814 (2001)
26. H. Grisaru, O. Palchik, A. Gedanken, V. Palchik, M.A. Slifkin, A.M. Weiss, Inorg. Chem. **42**, 7148 (2003)
27. J. Zhu, O. Palchik, S. Chen, A. Gedanken, J. Phys. Chem. B **104**, 7344 (2000)
28. H. Grisaru, V.G. Pol, A. Gedanken, I. Nowik, Eur. J. Inorg. Chem. **2004**, 1859 (2004)
29. Y.-L. Hsin, C.-F. Lin, Y.-C. Liang, K.C. Hwang, J.-C. Horng, J.-A. Ho, C.-C. Lin, J.R. Hwu, Adv. Funct. Mater. **18**, 2048 (2008)
30. B. Hu, S.-B. Wang, K. Wang, M. Zhang, S.-H. Yu, J. Phys. Chem. C **112**, 11169 (2008)
31. C.O. Kappe, Angew. Chem. Int. Ed. **43**(46), 6250 (2004)
32. D.S. Jacob, I. Genish, L. Klein, A. Gedanken, J. Phys. Chem. B Lett. **110**, 17711 (2006)
33. T. Yamauchi, Y. Tsukahara, K. Yamada, T. Sakata, Y. Wada, Chem. Mater. **23**, 75 (2011)
34. T. Yamamoto, H. Yin, Y. Wada, T. Kitamura, T. Sakata, H. Mori, S. Yanagida, Bull. Chem. Soc. Jpn. **77**, 757 (2004)
35. P.K. Sudeep, P.V. Kamat, Chem. Mater. **17**, 5404 (2005)
36. S. Tan, M. Erol, A. Attygalle, H. Du, S. Sukhishvili, Langmuir **23**, 9836 (2007)
37. Y. Niidome, K. Nishioka, H. Kawasaki, S. Yamada, Chem. Commun. **2376** (2003)
38. O.R. Miranda, N.R. Dollahon, T.S. Ahmadi, Cryst. Growth Des. **6**, 2747 (2006)
39. S. Eustis, H.-Y. Hsu, M.A. El-Sayed, J. Phys. Chem. B **109**, 4811 (2005)
40. K. Kurihara, J. Kizling, P. Stenius, J.H. Fendler, J. Am. Chem. Soc. **105**, 2574 (1983)
41. E. Leontidis, K. Kleitou, T. Kyprianidou-Leodidou, V. Bekiari, P. Lianos, Langmuir **18**, 3659 (2002)
42. E. Gachard, H. Remita, J. Khatouri, B. Keita, L. Nadjo, J. Belloni, New J. Chem. **22**, 1257 (1998)
43. R. Kissner, G. Welti, G. Geier, J. Chem. Soc. Dalton Trans. **10**, 1773 (1997)
44. A.-T. Le, P.T. Huy, T.Q. Huy, P.D. Cam, A.A. Kudrinskii, A.Y. Olenin, G.V. Lisichkin, Y.A. Krutyakov, Russ. Nanotechnol. **5**, 125 (2010)
45. N.L. Lala, R. Ramaseshan, L. Bojun, S. Sundarrajan, R.S. Barhate, L. Ying-jun, S. Ramakrishna, Biotechnol. Bioeng. **97**, 1357 (2007)

46. P.A. Muzalev, I.D. Kosobudskii, N.M. Ushakov, L.G. Panova, Perspekt. Mater. **84** (2011)
47. M.A. Kudryashev, A.I. Mashin, A.S. Tyurin, A.E. Fedosov, G. Chidichimo, G. De Filpo, Zh. Tekhn. Fiz. **81**, 95 (2011)
48. M.A. Kudryashev, A.I. Mashin, A.S. Tyurin, G. Chidichimo, G. De Filpo, Poverkhnost. Rentgenovskii, sinkhotronnye I neitronnye issledovaniya, **84** (2010)
49. Z. Zang, L. Zang, S. Wang, W. Chen, Y. Lei, Polymer **42**, 8315 (2001)
50. A.D. Pomogailo, G.I. Dzhardimalieva, V.N. Kestelman, *Macromolecular Metal Carboxylates and Their Nanocomposites* (Springer, Heidelberg, 2010)
51. Y. Lu, Y. Mei, M. Schrinner, M. Ballauff, M.W. Moller, J. Breu, J. Phys. Chem. C **111**, 7676 (2007)
52. A. Troupis, A. Hiskia, E. Papaconstantinou, Angew. Chem. Int. Ed. **41**, 1911 (2002)
53. S. Mandal, P.R. Selvakannan, R. Pasricha, M. Sastry, J. Am. Chem. Soc. **125**, 8440 (2003)
54. L. Yang, Y. Shen, A. Xie, J. Liang, S. Li, Q. Zhang, Eur. J. Inorg. Chem. **4658** (2006)
55. M.L. Marin, K.L. McGilvray, J.C. Scaiano, J. Am. Chem. Soc. **130**, 16572 (2008)
56. K.G. Stamplecoskie, J.C. Scaiano, Photochem. Photobiol. **88**, 762 (2012)
57. K. Esumi, T. Matsumoto, Y. Seto, T. Yoshimura, J. Colloid Interface Sci. **284**, 199 (2005)
58. C.S. Colley, D.C. Grills, N.A. Besley, S. Jockusch, P. Matousek, A.W. Parker, M. Towrie, N.J. Turro, P.M.W. Gill, M.W. George, J. Am. Chem. Soc. **124**, 14952 (2002)
59. S. Kapoor, T. Mukherjee, Chem. Phys. Lett. **370**, 83 (2003)
60. N. Kometani, H. Doi, K. Asami, Y. Yonezawa, Phys. Chem. Chem. Phys. **4**, 5142 (2002)
61. S. Eustis, G. Krylova, A. Eremenko, N. Smirnova, A.W. Schill, M. El-Sayed, Photochem. Photobiol. Sci. **4**, 154 (2005)
62. S. Jockusch, M.S. Landis, B. Freiermuth, N.J. Turro, Macromolecules **34**, 1619 (2001)
63. C.M. Gonzalez, Y. Liu, J.C. Scaiano, J. Phys. Chem. C **113**, 11861 (2009)
64. K.L. McGilvray, M.R. Decan, D. Wang, J.C. Scaiano, J. Am. Chem. Soc. **128**, 15980 (2006)
65. X. Zhu, B. Wang, F. Shi, J. Nie, Langmuir **28**, 14461 (2012)
66. M. Harada, E. Katagiri, Langmuir **26**, 17896 (2010)
67. M. Harada, N. Tamura, M. Takenaka, J. Phys. Chem. C **115**, 14081 (2011)
68. M. Harada, Y. Inada, Langmuir **25**, 6049 (2009)
69. P.V. Kamat, in *Semiconductor Nanoclusters – Physical, Chemical and Catalytic Aspects*, ed. by P.V. Kamat, D. Miesel (Elsevier Science, Amsterdam, 1997), pp. 237–259
70. D. Riassetto, F. Roussel, L. Rapenne, H. Roussel, S. Coindeau, O. Chaix, F. Micoud, M. Chatenet, M. Langle, J. Exp. Nanosci. **5**, 221 (2010)
71. S.K. Ghosh, S. Kundu, M. Mandal, S. Nath, T. Pal, J. Nanopart. Res. **5**, 577 (2003)
72. J.C. Scaiano, C. Aliaga, S. Maguire, D. Wang, J. Phys. Chem. B **110**, 12856 (2006)
73. Y.H. Ng, S. Ikeda, T. Harada, T. Sakata, H. Mori, A. Takaoka, M. Matsumura, Langmuir **24**, 6307 (2008)
74. X. Wang, J.C. Yu, H.Y. Yip, L. Wu, P.K. Wong, S.Y. Lai, Chem. Eur. J. **11**, 2997 (2005)
75. O. Carp, C.L. Huisman, A. Reller, Prog. Solid State Chem. **32**, 33 (2004)
76. D. Hufschmidt, D. Bahnemann, J.J. Testa, C.A. Emilio, M.I. Litter, J. Photochem. Photobiol. A **148**, 223 (2002)
77. R.D. Miller, Chem. Rev. **89**, 1359 (1989)
78. M. Sakamoto, T. Tachikawa, M. Fujitsuka, T. Majima, Chem. Mater. **20**, 2060 (2008)
79. T. Tamai, M. Watanabe, Y. Hatanaka, H. Tsujiwaki, N. Nishioka, K. Matsukawa, Langmuir **24**, 14203 (2008)
80. N.O. Yakimovich, N.V. Sapogova, L.A. Smirnova, A.P. Aleksandrov, T.A. Gracheva, A.V. Kirsanov, N.M. Bityurin, Khim. Fiz **27**, 61 (2008)
81. L.A. Smirnova, A.P. Aleksandrov, N.O. Yakimovich, N.V. Sapogova, A.V. Kirsanov, L.V. Soustov, N.M. Bityurin, Dokl. Akad. Nauk **400**, 779 (2005)
82. A.O. Rybaltovskii, A.A. Aksenov, V.I. Gerasimova, V.V. Zosimova, B.K. Popov, A.B. Solov'eva, P.S. Timashev, V.N. Bagratishvili, Sverkhkriticheskii fluidy: teoriya I praktika **3**, 50 (2008)

83. M. Kohsuke, Y. Miura, S. Shironita, M. Tomonari, N. Mimura, H. Yamashita, Stud. Surf. Sci. Catal. B **170**, 1319 (2007)
84. P. He, M. Zhang, D. Yang, J. Yang, Surf. Rev. Lett. **13**, 51 (2006)
85. K.P. Yu, W.Y. Yu, M.C. Kuo, Y.C. Liou, S.H. Chien, Appl. Catal. B **84**, 112 (2008)
86. S. Kundu, M. Mandal, S.K. Ghosh, T. Pal, J. Photochem. Photobiol. A **162**, 625 (2004)
87. N. Luo, L. Mao, L. Jiang, J. Zhan, Z. Wu, D. Wu, Mater. Lett. **63**, 154 (2009)
88. N.A. Agareva, A.P. Aleksandrov, L.A. Smirnova, N.M. Bityurin, Perspectivnye Materk **5** (2009)
89. M. Muniz-Miranda, J. Raman Spectrosc. **35**, 839 (2004)
90. J.C. Vinci, P. Bilski, R. Kotek, C. Chignell, Photochem. Photobiol. **86**, 806 (2010)
91. J. He, I. Ichinose, T. Kunitake, A. Nakao, Langmuir **18**, 10005 (2002)
92. P.V. Kamat, J. Phys. Chem. B **106**, 7729 (2002)
93. M.A. El-Sayed, Acc. Chem. Res. **34**, 257 (2001)
94. P.V. Kamat, M. Flumiani, G.V. Hartland, J. Phys. Chem. B **102**, 3123 (1998)
95. K. Kimura, J. Phys. Chem. **98**, 11997 (1994)
96. R.C. Jin, Y. Cao, E. Hao, G.S. Metraux, G.C. Schatz, C.A. Mirkin, Nature **425**, 487 (2003)
97. S.V. Karpov, V.V. Slabko, G.A. Chiganova, Colloid J. **64**, 425 (2002)
98. S.V. Karpov, A.L. Bas'ko, A.K. Popov, V.V. Slabko, Opt. Spectrosc. **95**, 241 (2003)
99. W.D. Bragg, V.A. Markel, W.T. Kim, K. Banerjee, M.R. Young, J.G. Zhu, R.L. Armstrong, V.M. Shalaev, Z.C. Ying, Y.E. Danilova, V.P. Safonov, J. Opt. Soc. Am. B **18**, 698 (2001)
100. A.K. Popov, J. Brummer, R.S. Tanke, G. Taft, M. Loth, R. Langlois, A. Wruck, R. Schmitz, Laser Phys. Lett. **3**, 546 (2006)
101. B.G. Ershov, Izv. AN, Ser. Khim. 1 (1999)
102. L.T. Bugaenko, M.G. Kuz'min, *Khimiya vysokikh energii* (Khimiya, Moscow), 1 (1988)
103. B.G. Ershov, Ros.khim. zh. (Ros. Khim. Zh. Ob-va im. D.I. Mendeleeva) **45**, 20 (2001)
104. A.B. Zezin, V.B. Rogacheva, S.P. Valueva, N.I. Nikonorova, M.F. Zansokhova, A.A. Zezin, Russ. Nanotechnol. **191** (2006)
105. A. Henglein, M. Gutierrez, E. Janata, B.G. Ershov, J. Phys. Chem. **96**, 4598 (1992)
106. A. Henglein, D. Meisel, Langmuir **14**, 7392 (1998)
107. B.G. Ershov, E. Janata, A. Henglein, Radiat. Phys. Chem. **39**, 123 (1992)
108. B.G. Ershov, E. Janata, A. Henglein, J. Phys. Chem. **97**, 339 (1993)
109. B.G. Ershov, N.L. Sukhov, D.L. Troitskii, Radiat. Phys. Chem. **39**, 127 (1992)
110. D.A. Troitskii, N.L. Sukhov, B.G. Ershov, A.V. Gordeev, Khim. Vysok. Energii **29**, 218 (1994)
111. M. Michaelis, A. Henglein, J. Phys. Chem. **96**, 4719 (1992)
112. B.G. Ershov, E. Janata, M. Michaelis, A. Henglein, J. Phys. Chem. **95**, 8996 (1991)
113. A. Radosavljević, D. Božanić, N. Bibić, M. Mitrić, Z. Kačarević-Popović, J. Nedeljković, J. Appl. Polym. Sci. **125**, 1244 (2012)
114. Y.-O. Kang, S.-H. Choi, A. Gopalan, K.-P. Lee, H.-D. Kang, Y.S. Song, J. Appl. Polym. Sci. **100**, 1809 (2006)
115. S.-H. Choi, M.S. Choi, K.P. Lee, H.D. Kang, J. Appl. Polym. Sci. **91**, 2335 (2004)
116. M.R. Karim, K.T. Lim, C.J. Lee, M.T. Bhuiyan, H.J. Kim, L.S. Park, M.S. Lee, J. Polym. Sci. Part A Polym. Chem. **45**(24), 5741 (2007)
117. H.L. Abd El-Mohdy, J. Polym. Res. **20**, 177 (2013)
118. R. Singh, D. Singh, J. Mater. Sci. Mater. Med. **23**, 2649 (2012)
119. Z. Ajji, I. Othman, J.M. Rosiak, Nucl. Instrum. Methods Phys. Res. B **229**, 375 (2005)
120. N. Leventis, C. Sotiriou-Leventis, G. Zhang, A.-M.M. Rawashdeh, Nano Lett. **2**, 957 (2002)
121. G. Piccaluga, A. Corrias, G. Ennas, A. Musinu, *Sol-Gel Preparation and Characterization of Metal-Silica and Metal Oxide-Silica Nanocomposites*. Materials Science Foundation (Trans Tech Publications, Switzerland, 2000)
122. J.F. Hund, M.F. Bertino, G. Zhang, C. Sotiriou-Leventis, N. Leventis, A. Tokuhiro, J. Farmer, J. Phys. Chem. B **107**, 465 (2003)

123. M.F. Bertino, J.F. Hund, G. Zhang, C. Sotiriou-Leventis, A.T. Tokuhiro, N. Leventis, J.Sol-Gel Sci. Technol. **30**, 43 (2004)
124. M. Mostafavi, Y.P. Lin, P. Pernot, J. Belloni, Radiat. Phys. Chem. **59**, 49 (2000)
125. A.H. Souici, N. Keghouche, J.A. Delaire, H. Remita, M. Mostafavi, Chem. Phys. Lett. **422**, 25 (2006)
126. A.L. Pan, J.G. Ma, X.Z. Yan, B.S. Zou, J. Phys. Condens. Matter **16**, 3229 (2004)
127. H.L. Su, J. Han, Q. Dong, D. Zhang, Q.X. Guo, Nanotechnology **19**, 025601 (2007)
128. S. Ghosh, S.C. Bhattacharya, A. Saha, Anal. Bioanal. Chem. **397**, 1573 (2010)
129. A.H. Souici, N. Keghouche, J.A. Delaire, H. Remita, A. Etcheberry, M. Mostafavi, J. Phys. Chem. C **113**, 8050 (2009)
130. S.-q. Chang, B. Kang, Y.-d. Da, H.-x. Zhang, D. Chen, Nanoscale Res. Lett. **6**, 591 (2011)
131. X. Michalet, F.F. Pinaud, L.A. Bentolila, J.M. Tsay, S. Doose, J.J. Li, G. Sundaresan, A.M. Wu, S.S. Gambhir, S. Weiss, Science **307**, 538 (2005)
132. S. Ghosh, A. Priyam, A. Chatterjee, A. Saha, J. Nanosci. Nanotechnol. **8**, 5952 (2008)
133. N.A. Melosh, A. Boukai, F. Diana, B. Gerardot, A. Badolato, P.M. Pelroff, J.R. Heath, Science **300**, 112 (2003)
134. K.R. Reddy, K.-P. Lee, A.I. Gopalan, M.S. Kim, A.M. Showkat, Y.C. Nho, J. Polym, Sci. Part A Polym. Chem. **44**, 3355 (2006)
135. A. Henglein, J. Phys. Chem. B **104**, 2201 (2000)
136. Q. Wan, C.L. Lin, X.B. Yu, T.H. Wang, Appl. Phys. Lett. **83**, 124 (2004)
137. Z. Zhang, T.M. Nenoff, K. Leung, S.R. Ferreira, J.Y. Huang, D.T. Berry, P.P. Provencio, R. Stumpf, J. Phys. Chem. C **114**, 14309 (2010)
138. Z. Zhang, T.M. Nenoff, J.Y. Huang, D.T. Berry, P.P. Provencio, J. Phys. Chem. C **113**, 1155 (2009)
139. C.M. Doudna, M.F. Bertino, F.D. Blum, A.T. Tokuhiro, D. Lahiri-Dey, S. Chattopadhyay, J. Terry, J. Phys. Chem. B **107**, 2966 (2003)
140. K. Roy, S. Lahiri, Green Chem. **8**, 1063 (2006)
141. K. Roy, S. Lahiri, Anal. Chem. **80**, 7504 (2008)
142. K.S. Suslick, D.A. Hammerton, R.E. Cline, J. Am. Chem. Soc. **108**, 5641 (1986)
143. K.S. Suslick, S.B. Choe, A.A. Cichowlas, M.W. Grinstaff, Nature **353**, 414 (1991)
144. N.A. Dhas, C.P. Raj, A. Gedanken, Chem. Mater. **10**, 1446 (1998)
145. K. Okitsu, A. Yue, S. Tanabe, H. Matsumoto, Y. Yobiko, Y. Yoo, Bull. Chem. Soc. Jpn. **75**, 2289 (2002)
146. R.A. Caruso, M. Ashokkumar, F. Grieser, Langmuir **18**, 7831 (2002)
147. A. Roucoux, J. Schulz, H. Patin, Chem. Rev. **102**, 3757 (2002)
148. K. Okitsu, M. Ashokkumar, F. Grieser, J. Phys. Chem. B **109**, 20673 (2005)
149. T. Prozorov, R. Prozorov, K.S. Suslick, J. Am. Chem. Soc. **126**, 13890 (2004)
150. D. Radziuk, D. Grigoriev, W. Zhang, D. Su, H. Mo¨hwald, D. Shchukin, J. Phys. Chem. C **114**, 1835 (2010)
151. K. Vinodgopal, Y. He, M. Ashokkumar, F. Grieser, J. Phys. Chem. B **110**, 3849 (2006)
152. S. Anandan, F. Grieser, M. Ashokkumar, J. Phys. Chem. C **112**, 15102 (2008)
153. Y. Mizukoshi, E. Takagi, H. Okuno, Y. Maeda, Y. Nagata, Ultrason. Sonochem. **8**, 1 (2001)
154. J. Reisse, T. Caulier, C. Deckerkheer, O. Fabre, J. Vandercammen, J.L. Delplancke, R. Winand, Ultrason. Sonochem. **3**, S147 (1996)
155. A. Durant, J.L. Delplancke, R. Winand, J. Reisse, Tetrahedron Lett. **36**, 4257 (1995)
156. X.F. Qiu, J.Z. Xu, J.M. Zhu, J.J. Zhu, S. Xu, H.Y. Chen, J. Mater. Res. **18**, 1399 (2003)
157. L.P. Jiang, A.N. Wang, Y. Zhao, J.R. Zhang, J.J. Zhu, Inorg. Chem. Commun. **7**, 506 (2004)
158. I. Haas, S. Shanmugam, A. Gedanken, J. Phys. Chem. B **110**, 16947 (2006)
159. J. Rae, M. Ashokkumar, O. Eulaerts, C.V. Sonntag, J. Reisse, F. Grieser, Ultrason. Sonochem. **12**, 325 (2005)
160. G. Cárdenas-Trivinõ, R.A. Segura, J. Reyes-Gasga, Colloid Polym. Sci. **282**, 1206 (2004)
161. I. Szaraz, W. Forsling, Langmuir **17**, 3987 (2001)
162. C.M. Koo, H.T. Ham, M.H. Choi, S.O. Kim, I.J. Chung, Polymer **44**, 681 (2003)

163. A. Nemamcha, J.-L. Rehspringer, D. Khatmi, J. Phys. Chem. B **110**, 383 (2006)
164. T. Alammar, A.-V. Mudring, J. Mater. Sci. **44**, 3218 (2009)
165. T. Alammar, A. Birkner, O. Shekhah, A.-V. Mudring, Mater. Chem. Phys. **120**, 109 (2010)
166. T. Alammar, A.-V. Mudring, ChemSusChem **4**, 1796 (2011)
167. S. Lei, K. Tang, Z. Fang, H. Zheng, Cryst. Growth Des. **6**, 1757 (2006)
168. J. Zhang, J. Du, B. Han, Z. Liu, T. Jiang, Z. Zhang, Angew. Chem. Int. Ed. **45**, 1116 (2006)
169. R. Abu-Much, A. Gedanken, Chem. Eur. J. **14**, 10115 (2008)
170. L. Xu, L.-P. Jiang, J.-J. Zhu, Nanotechnology **20**, 045605 (2009)
171. B.M. Teo, S.W. Prescott, M. Ashokkumar, F. Grieser, Ultrason. Sonochem. **15**, 89 (2008)
172. V. Belova, H. Mo¨hwald, D.G. Shchukin, Langmuir **24**, 9747 (2008)
173. G. Qiu, Q. Wang, M. Nie, J. Appl. Polym. Sci. **102**, 2107 (2006)
174. Y. Liao, Q. Wang, H. Xia, Polym. Int. **50**, 207 (2001)
175. S. Manickam, in *Theoretical and Experimental Sonochemistry Involving Inorganic Systems*, ed. by Pankaj, M. Ashokkumar (Springer, Heidelberg, 2011), pp. 191–211
176. H. Biederman, *Plasma Polymer Films* (Imperial College Press, London, 2004)
177. A. Biswas, Z. Marton, J. Kanzow, J. Kruse, V. Zaporojtchenko, F. Faupel, T. Strunskus, Nano Lett. **3**, 1 (2003)
178. H. Takele, H. Greve, C. Pochstein, V. Zaporojtchenko, F. Faupel, Nanotechnology **17**, 3499 (2006)
179. J. Zheng, R. Yang, L. Xie, J. Qu, Y. Liu, X. Li, Adv. Mater. **22**, 1451 (2010)
180. A. Borras, A. Barranco, F. Yubero, A.R. Gonzalez-Elipe, Nanotechnology **17**, 3518 (2006)
181. A.D. Pomogailo, V.N. Kestelman, *Metallopolymer Nanocomposites* (Springer, Berlin/Heidelberg, 2005)
182. A. Heilmann, J. Werner, M. Kelly, B. Holloway, E. Kay, Appl. Surf. Sci. **115**, 365 (1997)
183. C. Laurent, E. Kay, J. Appl. Phys. **65**, 1717 (1989)
184. A. Choukourov, P. Solar, O. Polonskyi, J. Hanus, M. Drabik, O. Kylian, E. Pavlova, D. Slavinska, H. Biederman, Plasma Process. Polym. **7**, 25 (2010)
185. E. Dilonardo, A. Milella, F. Palumbo, G. Capitani, R. d'Agostino, F. Fracassi, Plasma Process. Polym. **7**, 51 (2010)
186. F. Fracasssi, R. d'Agostino, F. Palumbo, F. Bellucci, T. Monetta, Thin Solid Films **264**, 40 (1995)
187. H. Biederman, L. Martinu, in *Plasma Deposition, Treatment, and Etching of Polymers*, ed. by R. d'Agostino (Academic, San Diego, 1990), p. 269
188. H. Biederman, O. Polonskyi, M. Drabik, O. Kylian, J. Kousal, J. Hanus, A. Choukourov, P. Solar, A. Serov, D. Slavinska, 30th ICPIG, August 28th–September 2nd 2011, Belfast, Northern Ireland, UK
189. P.-G. Reinhard, E. Suraud, *Introduction to Cluster Dynamics* (Wiley-VCH, Mörlenbach, 2004)
190. S.H. Baker, S.C. Thornton, K.W. Edmonds, M.J. Maher, C. Norris, C. Binns, Rev. Sci. Instrum. **71**, 3178 (2000)
191. T. Peter, S. Rehders, U. Schu¨rmann, T. Strunskus, V. Zaporojtchenko, F. Faupel, J. Nanopart. Res. **15**, 1710 (2013)
192. L. Ravagnan, G. Divitini, S. Rebasti, M. Marelli, P. Piseri, P. Milani, J. Phys. D. Appl. Phys. **42**, 082002 (2009)
193. A. Kubono, N. Okui, Prog. Polym. Sci. **19**, 389 (1994)
194. H.T. Beyene, V.S.K. Chakravadhanula, C. Hanisch, M. Elbahri, T. Strunskus, V. Zaporojtchenko, L. Kienle, F. Faupel, J. Mater, Science **45**, 5865 (2010)
195. H.T. Beyene, V.S.K. Chakravadhanula, C. Hanisch, T. Strunskus, V. Zaporojtchenko, M. Elbahri, F. Faupel, Plasmonics **7**, 107 (2012)
196. H. Biederman, Vacuum **59**, 594 (2000)
197. U. Schu¨rmann, H. Takele, V. Zaporojtchenko, F. Faupel, Thin Solid Films **515**, 801 (2006)
198. N. Alissawi, V. Zaporojtchenko, T. Strunskus, I. Kocabas, V.S.K. Chakravadhanula, L. Kienle, D. Garbe-Schönberg, F. Faupel, Gold Bull. **46**, 3 (2013)

199. K. Baba, T. Okuno, M. Miyagi, Appl. Phys. Lett. **62**, 437 (1993)
200. M. Schierhorn, L.M. Liz-Marzan, Nano Lett. **2**, 13 (2002)
201. G. Gonzalo, D. Babonneau, C.N. Afonso, J.-P. Barnes, J. Appl. Phys. **96**, 5163 (2004)
202. E. Cottancin, J. Lerme, M. Gaudry, M. Pellarin, J.-L. Vialle, M. Broyer, Phys. Rev. B **62**, 5179 (2000)
203. A. Kulkarni, V.S.K. Chakravadhanula, V. Duppel, D. Meyners, V. Zaporojtchenko, T. Strunskus, L. Kienle, E. Quandt, F. Faupel, J. Mater. Sci. **46**, 4638 (2011)
204. N. Alissawi, T. Peter, T. Strunskus, C. Ebbert, G. Grundmeier, F. Faupel, J. Nanopart. Res. **15**, 2080 (2013)
205. A.V. Simakin, V.V. Voronov, G.A. Shafeev, Trudy institute obshchei fiziki im. A.M. Prokhorova **60**, 83 (2004)
206. T.X. Phuoc, Y. Soong, M.K. Chyu, Optics Lasers Eng. **45**, 1099 (2007)
207. I.V. Kavetskaya, T.V. Voloshina, V.A. Karnavskii, V.I. Krasovskii, Kondensirovannye sredy I mezhfaznye granitsy **11**, 53 (2009)
208. H.Y. Kwong, Y.W. Wong, K.H. Wong, J. Appl. Phys. **102**, 114303 (2007)
209. T. Tsuji, D.H. Thang, Y. Okazaki, M. Nakanishi, Y. Tsuboi, M. Tsuji, Appl. Surf. Sci. **254**, 5224 (2008)
210. S. Barcikowski, F. Devesa, K. Moldenhauer, J. Nanopart. Res. **11**, 1883 (2009)
211. S. Petersen, S. Barcikowski, Adv. Funct. Mater. **19**, 1 (2009)
212. S. Besner, A.V. Kabashin, F.M. Winnik, M. Meunier, J. Phys. Chem. C **113**, 9526 (2009)
213. S. Salmaso, P. Caliceti, V. Amendola, M. Meneghetti, J.P. Magnusson, G. Pasparakis, C. Alexander, J. Mater. Chem. **19**, 1608 (2009)
214. Y. Takeda, T. Kondow, F. Mafune, J. Phys. Chem. B **110**, 2393 (2006)
215. S.I. Mikulitskii, V.Y. Khomich, V.A. Shmakov, V.A. Yamshchikov, Russ. Nanotechnol. **6**, 65 (2011)
216. M.S. Hu, H.L. Chen, C.H. Shen, L.S. Hong, B.R. Huang, K.H. Chen, L.C. Chen, Nat. Mater. **5**, 102 (2006)
217. W. Guo, M. Zhang, A. Banerjee, P. Bhattacharya, Nano Lett. **10**, 3355 (2010)
218. M.L. Wang, C.G. Huang, Y.G. Cao, Q.J. Yu, W. Guo, Q.L. Liu, J.K. Liang, M.C. Hong, Nanotechnology **20**, 285311 (2009)